Journal of Nanobiotechnology

RESEARCH

Open Access

Co-encapsulation of norcantharidin prodrugs and lomitapide in nanoparticles to regulate CCL4 expression by inhibiting Wnt/β-catenin pathway for improved anti-tumor immunotherapy

Feng Zhao[1†], Liming Gong[2†], Ping Wang[1†], Dong Chen[3], Shijie Cao[4], Feifei Yang[5], Manqing Tang[1], Yuanyuan Meng[1], Yuming Wang[1], Lin Miao[4*], Yunfei Li[1,6*] and Wei Huang[2*]

Abstract

In the absence of tumor antigen specificity, direct chemokine administration carries the risk of significant "on-target, off-tumor" toxicities, highlighting the need for small-molecule approaches with reduced immunogenicity. This study investigates the synergistic potential of norcantharidin (NCTD) and lomitapide (lomi) in selectively restoring CCL4 expression by deactivating the tumor intrinsic β-catenin pathway. Due to its similar lipophilicity to lomi and potential to suppress β-catenin, NCTD prodrug (C12) was selected to be co-encapsulated with lomi in a nanoparticle-mediated co-delivery system (NP"C12 + lomi"). The NP"C12 + lomi" formulation exhibited a high encapsulation rate, uniform particle size, and suitability for therapeutic use. It effectively inhibited the proliferation of 4T1 cells and restored CCL4 expression. In both primary breast tumor and surgically resected tumor mouse models, NP"C12 + lomi" significantly increased the proportion of $CD8^+$ cells in primary tumors, blood, and lung metastases, approximately doubling their presence. This led to a prolongation of median survival in mice to 59 days. Furthermore, when combined with an immune checkpoint inhibitor, NP"C12 + lomi" substantially inhibited tumor growth and lung metastasis without affecting body weight or causing major tissue or organ damage. This was attributed to the controlled dissociation of the nanoparticle and the subsequent modulation of C12 and lomi, which mitigated CCL4-related toxicity. This study provides valuable insights into the safe production of chemokines

[†]Feng Zhao, Liming Gong and Ping Wang equally contributed to this work.

*Correspondence:
Lin Miao
mmmlin@tjutcm.edu.cn
Yunfei Li
liyunfei@tjutcm.edu.cn
Wei Huang
huangwei@imm.ac.cn

Full list of author information is available at the end of the article

using a small-molecule pair through a nanosystem and presents a robust chemo-immunological cascade therapy strategy, demonstrating significant efficacy against malignant metastatic tumors.

Graphical abstract

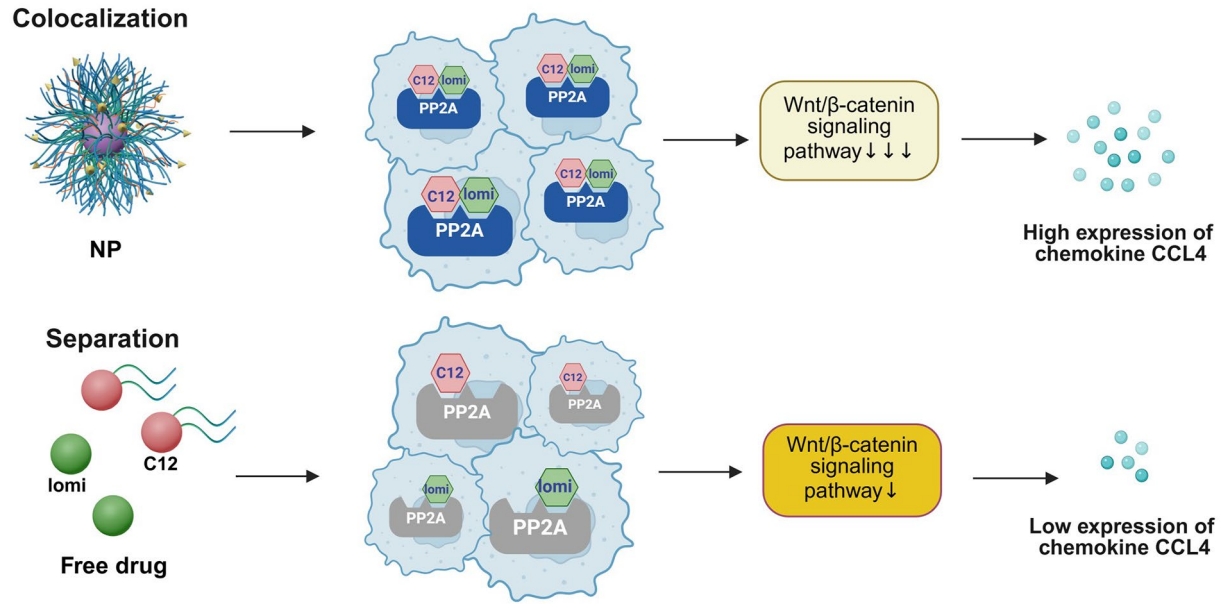

Keywords Chemokine immunotherapy, Small molecule strategy, β-catenin inhibition, Nanoparticle colocalization, Metastasis mitigation

Introduction

Chemokines like CCL4 [1] and CXCL9/10 [2, 3] have been shown to facilitate the infiltration of crucial immune cells and synergize with immune checkpoint inhibitors (ICIs). The existing literature extensively details the role of chemokines in facilitating the infiltration of various immune cells into the tumor microenvironment(TME) [3]. Specifically, chemokine CCL4, which acts as a ligand for CCR5, is secreted by multiple immune cells, including neutrophils, T cells, monocytes, and B cells [4]. Studies have shown that elevated levels of CCL4 enhance the recruitment of $CD8^+$ T cells, thereby augmenting potent anti-tumor immune responses [4–6]. Despite its emerging role in immunotherapy, chemokine therapy faces several challenges. The low molecular mass and short half-life of chemokines require high dosages for effective administration in the TME, which can lead to immune-related adverse effects (irAEs), such as cytokine release syndrome [7–9]. For example, IL-12 demonstrated high toxicity in a phase II trial involving intravenous administration, tragically leading to the fatalities of two out of seventeen patients [10]. These issues present substantial barriers to translating chemokine therapy into a widely applicable clinical strategy.

Given the limitations of chemokine-based therapies, small-molecule immune modulators represent a promising alternative. These molecules are more stable, can be administered orally, and often demonstrate better pharmacokinetic properties, such as enhanced tumor penetration and a reduced risk of immunogenicity [11, 12]. Notably, small molecules can potentially circumvent the adverse effects associated with biologic therapies, offering a more cost-effective and safer approach to cancer immunotherapy. Thus, small-molecule immune modulators hold the potential to circumvent the limitations associated with biologics and could effectively serve as adjuncts to clinical ICIs [13, 14].

In melanoma treatment, the activation of the Wnt/β-catenin signaling pathway has been found to be negatively correlated with CCL4 gene expression [2]. Targeting the tumor cell-intrinsic β-catenin pathway presents a promising strategy for restoring CCL4 expression and enhancing immunological cell infiltration [1, 15–17]. However, targeting β-catenin directly has limitations, such as the challenge of effective delivery and the need for high doses to achieve therapeutic outcomes without causing toxicity. Norcantharidin (NCTD) diacid, a well-established inhibitor of protein phosphatase 1/2A (PP1/2A), associates with the β-catenin destruction complex, promoting the ubiquitin-dependent degradation of β-catenin [18–21]. Despite its potential, the efficacy of NCTD is limited by its rapid clearance from the TME, poor cell

internalization, and potential systemic toxicity. Lomitapide (lomi), an FDA-approved lipid-lowering agent, has been repositioned to inhibit PP2A, a critical regulator of the β-catenin pathway [22, 23]. The combination of NCTD and lomi is strategically chosen because of their synergistic effects on β-catenin deactivation, which could restore CCL4 expression in tumor cells. Our preliminary investigations showed that while NCTD [24] and lomi individually exhibited modest effects on β-catenin deactivation, their combined use significantly reduced cancer stemness and increased CCL4 expression. These findings support further exploration of this dual small molecule regimen to enhance β-catenin inhibition in cancer treatment.

Beyond enabling precise targeting of drugs to tumor sites and malignant cells, nanoparticle (NP) formulations offer an ideal platform for colocalizing two molecules to exert synergistic effects, wherein synergistic drug combinations are physically integrated to enhance cancer treatment outcomes [25]. In this study, we propose a "synergism-triggered nanoparticle" to enhance CCL4 expression in tumor cells. The "synergism-triggered nanoparticle" designed to modulate the release and activity of therapeutic agents in response to specific triggers, optimizing the local concentration of chemokines while minimizing systemic toxicity. This system leverages the synergistic combination of NCTD and lomi to enhance the activation of immune cells by restoring CCL4 expression in the TME. The advantages of this nanoparticle-mediated combinatorial approach include: (I) the clinical safety profiles of both NCTD and lomi being well-established; (II) synergism allowing for lower drug doses and reduced side effects [25] and (III) the NP-based integration that confines CCL4 expression to the desired site, preventing "on-target, off-site" toxicity from unintended chemokine distribution in vivo. This strategic framework highlights the pivotal role of small-molecule agents in modulating immune cells, offering significant clinical implications for broad applicability and feasibility in cancer immunotherapy (Fig. 1).

Results

Synergistic induction of robust CCL4 production via β-Catenin suppression by "NCTD + lomi" synergism

Despite the exponential increase in studies using nanocarriers to co-deliver drug combinations since 1999 [25], most research based on this de novo approach remains confined to preclinical stages, with Vyxeos® being the only approved example to date [26]. In this context, we sought to explore the underlying potentials of the "NCTD + lomi" regimen, both of which are already marketed. NCTD has been shown to suppress TNBC cancer stem cell (CSC)-like properties by deactivating β-catenin pathway [24]. However, its single use does not satisfactorily enhance CCL4 expression in tumor cells. Given that antineoplastic medicines with similar effects are often administered in combination, small molecules eradicating CSC-like properties were presumed to assist NCTD in restoring CCL4. From a library of FDA-approved drugs, the lipid-lowering agent lomi was found to have the potential to attenuate CSC-like properties [23] and was thus utilized as an adjunct to NCTD.

Regardless of the use of radiation, chemotherapy, or immunotherapy, TNBC features a poor prognosis and low five-year survival rate, and is deemed an inflamed-cold tumor. The mouse TNBC 4T1 cell line was chosen as the cold tumor model, which exhibits limited immune infiltration and low response to anti-PD1 treatment [27]. As shown in Fig. 2A, the "NCTD + lomi" combination strategy was designed to treat 4T1 cells over four generations continuously. Compared to single-agent treatments, the combination showed impressive synergism, diminishing active β-catenin levels from the 2nd generation and enhancing E-cadherin levels by the 4th generation (Fig. 2B). This was further validated by quantitative analysis of Western blot (WB) data from three independent experiments, with the results represented in the column charts (Supplementary Fig. 1). The data consistently showed significant reductions in active β-catenin and increased E-cadherin expression in the combination treatment group, highlighting the enhanced therapeutic efficacy. Furthermore, we utilized MSAB, a small molecule known to directly bind β-catenin and promote its proteasome-mediated degradation, thereby specifically inhibiting the Wnt/β-catenin pathway. Previous studies have demonstrated that MSAB can effectively suppress the growth of Wnt/β-catenin-dependent cancer cells, highlighting its potential as a therapeutic strategy [28]. To further investigate the mechanism underlying the enhanced antitumor effect of combination of NCTD and lomi, we performed WB analysis to evaluate β-catenin signaling. The results revealed that cells treated for four generations with NCTD and lomi markedly reduced the expression levels of both total and active β-catenin. Notably, this inhibitory effect was comparable to that of MSAB (Supplementary Fig. 2). These findings suggest that combination of NCTD and lomi may suppress tumor progression, at least in part, by modulating the Wnt/β-catenin signaling pathway, in a manner similar to MSAB. To investigate whether the treatment affected the cancer stem-like cell population, we evaluated the mRNA expression levels of CD44 and CD24, two well-established markers used to characterize breast cancer stem cells. In particular, the $CD44^{+}/CD24^{-/low}$ phenotype has been widely associated with breast cancer stemness, self-renewal, tumorigenicity, and therapeutic resistance [29]. The expression of CD44 was significantly reduced, while CD24 expression was elevated after treatment, leading to

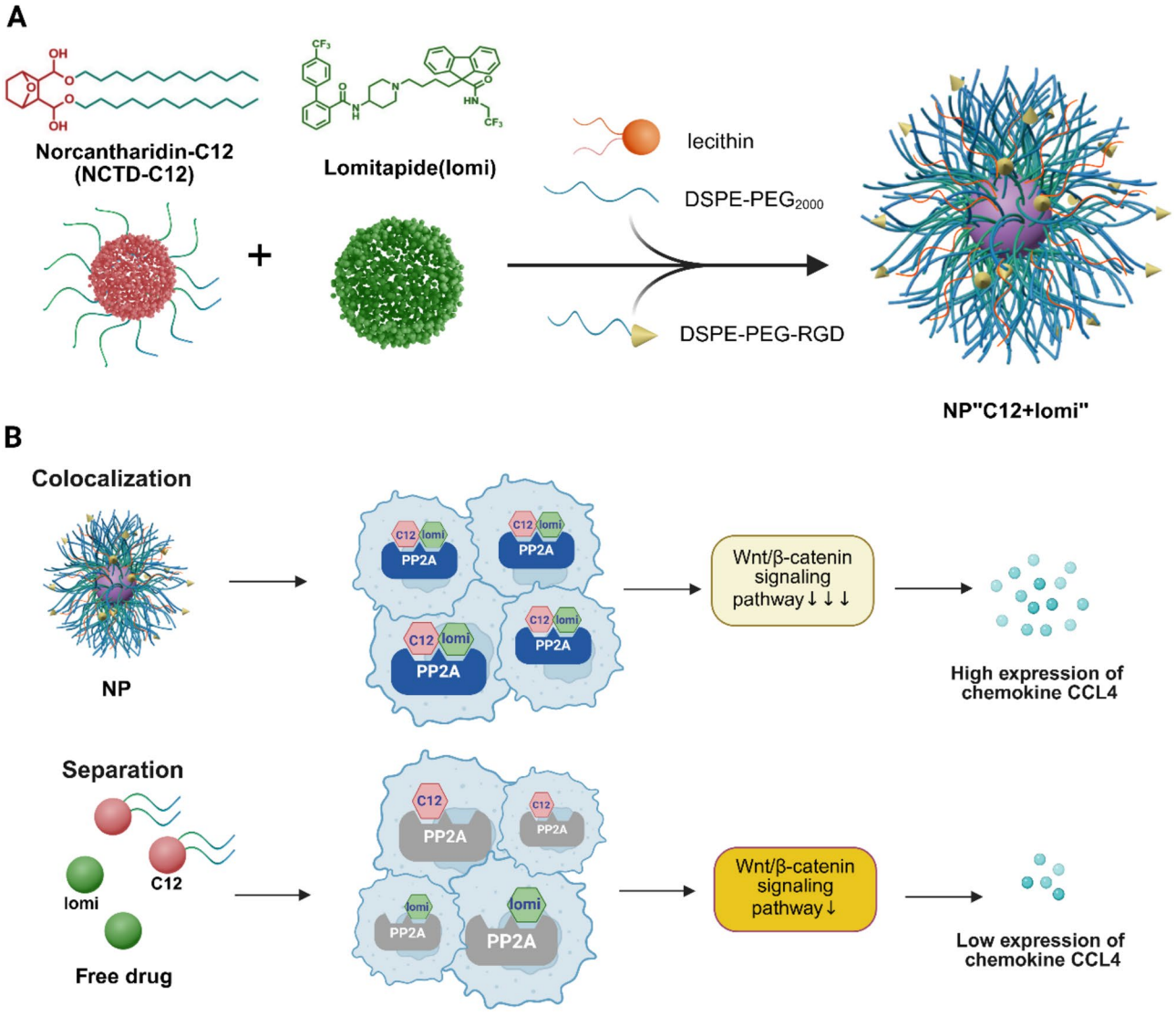

Fig. 1 Design and mechanism of "NCTD-C12 + lomi" nanoparticle to robust CCL4 production via Wnt/β-Catenin signaling pathway suppression.(**A**) Construction of the nano drug delivery system. This panel illustrates the assembly of a nanoscale drug delivery system, which encapsulates two distinct therapeutic agents within a single nanocarrier. (**B**) Regulation of chemokine CCL4 expression via Wnt/β-Catenin signaling pathway modulation. In the nanocarrier system, the encapsulated drugs act synergistically to inhibit the activity of the PP2A protein, leading to a coordinated downregulation of the Wnt/β-Catenin signaling pathway. This synergistic inhibition is correlated with an elevated expression of chemokine CCL4, suggesting a potentiated therapeutic response due to the nanoparticle delivery approach. In contrast, when the two drugs are administered in their free state, they do not exhibit a synergistic effect on the inhibition of PP2A protein or the downregulation of the Wnt/β-Catenin signaling pathway. The lack of synergy results in a lower expression of CCL4, indicating a diminished therapeutic impact compared to the nanoparticle-mediated delivery. Created in https://BioRender.com

an increased CD24/CD44 ratio (Supplementary Fig. 3). This trend suggests a reduction in the stemness phenotype of breast cancer cells. The shift in the CD24/CD44 ratio suggests a reduction in stem-like characteristics, which could indicate a decrease in the cancer stem cell population after treatment. Both proteins were important markers for cancer stemness, and thus "NCTD + lomi" elicited more robust CCL4 expressions than its individual components (Fig. 2C). Preliminary evidence indicates that the combined use of the two drugs results in a five-fold increase in the expression of the chemokine CCL4 compared to the use of either drug alone (Fig. 2D). Inappropriate activation of the Wnt pathway drives tumor formation [30]. Similarly, the "NCTD + lomi" combination also exhibited a strong inhibitory effect on three-dimensional (3D) soft agar long-term colony formation by 4T1 cells (Fig. 2E, F), implicating reduced oncogenesis of individual CSC at the distant organ. As β-catenin activation is strongly associated with CSC-like properties, the results revealed a deactivated β-catenin status due to the combination treatment. Immune evasion in many cancers is also associated with β-catenin activation,

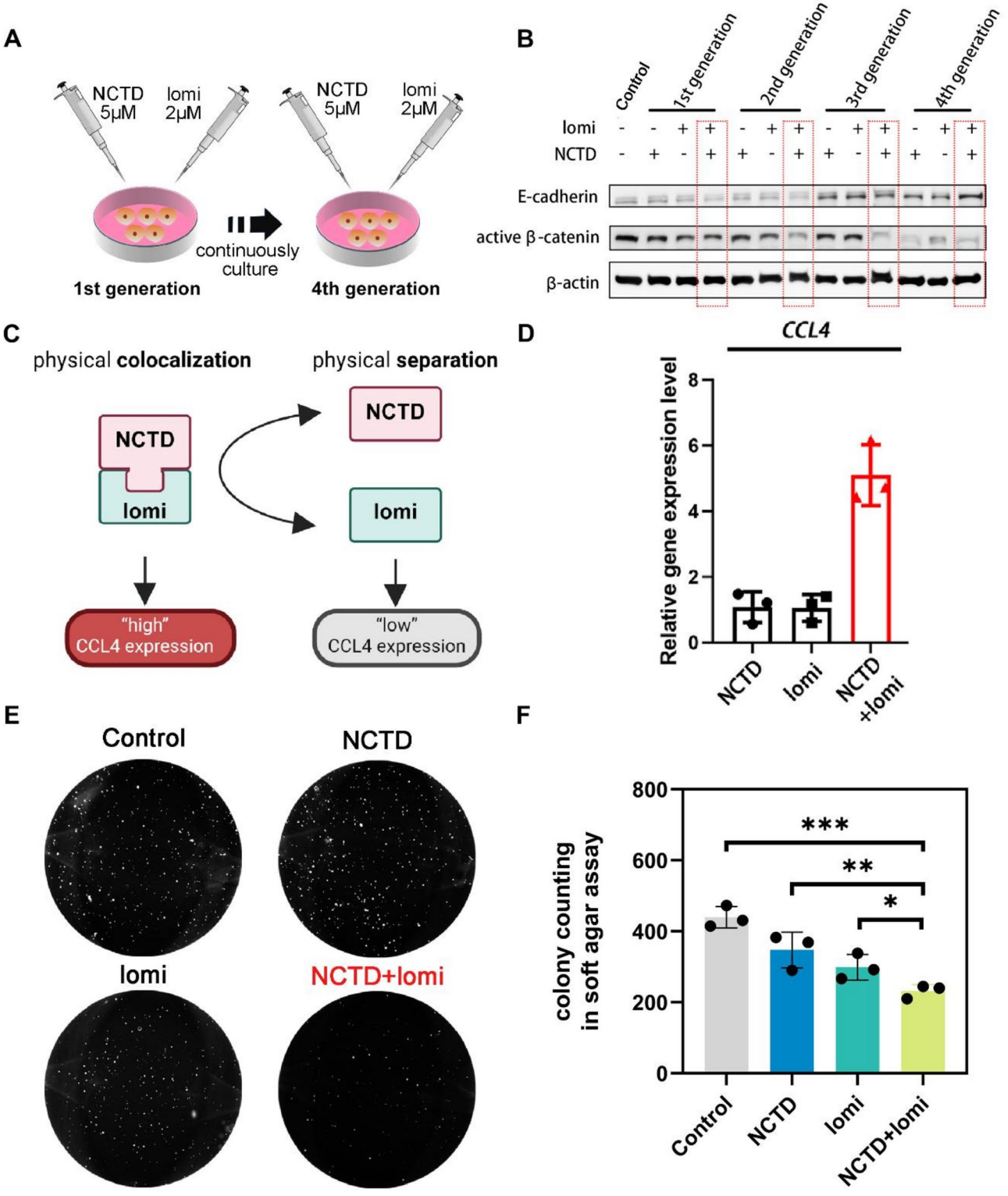

Fig. 2 The synergism of two small-molecule combination to elicit CCL4 expression via deactivating β-catenin. (**A**) Schematic illustration of NCTD (5 μM) and lomi (2 μM) co-exposure from the 1st generation 4T1 cells to the 4th generation 4T1 cells. (**B**) Western blotting results of E–cadherin and active β-catenin levels of 4 generations 4T1 cells after lomi + NCTD co-exposure. (**C**) Schematic representation illustrating the synergistic effect of NCTD and lomi on the regulatory mechanism of CCL4 expression. (**D**) qPCR analysis of CCL4 mRNA expressions on 4T1 cells after exposure to the single- and dual-drug. (**E**) Colony formation of 4T1 cells on soft agar. Anchorage-independent cell growths from control, NCTD, lomi and NCTD + lomi groups were evaluated by soft agar assay. The representative pictures were presented by Colony formation of 4T1 cells on soft agar. (**F**) Quantitative analysis of 4T1 cells colony formation. The data were presented as mean ± SD ($n = 3$). *$P < 0.05$; **$P < 0.01$; ***$P < 0.001$

which inhibits cytokines/chemokines gene expression. Chemokine CCL4 plays a critical role in recruiting immune cells, including $CD8^+$ T cell infiltration [1, 31, 32]. Thus, based on these pilot study results, we proposed a small molecule strategy utilizing NCTD and lomi to elicit CCL4 expression in TME.

In a combinatorial regimen, the efficacy magnitude is generally depicted as either simple additivity or super-additivity (synergism). Traditionally, the primary role of developing co-delivery NPs has been to avoid the chemoresistance of tumor cells through various mechanisms, with synergism among drugs not being the top priority [33, 34]. However, in our case, the super synergism demonstrated by the "NCTD + lomi" combination far exceeded from their individual potencies. This suggests that their efficacy in deactivating β-catenin will diminish after NP physical disassociation, thereby minimizing impairment to somatic stem cells. Collectively, this level of synergism provided an excellent opportunity to modulate CCL4 expression by combining or separating the molecule pair.

Design and assessment of NCTD-lipid prodrugs

NCTD has antitumor effects due to its structure, which contains an oxygenated six-membered ring and dicarboxylic anhydride. However, it is prone to ring opening and hydrolysis in the aqueous environment, ultimately transforming into NCTD diacid. The limited half-life of NCTD diacid restricts its potential applications in cancer therapy [35]. In contrast, lomi is a hydrophobic molecule with a water solubility as low as 5.267×10^{-8} mg L^{-1} [36]. The drastic differences in their physiochemical properties can lead to the premature release of NCTD, which may compromise the synergism needed to restore chemokine CCL4 in vivo. Precisely controlling the release profile of NCTD to match that of lomi is important. To optimize these unfavorable physicochemical properties, a prodrug strategy was adopted for NCTD in present study.

Despite the two carboxyl groups in NCTD diacid causing high polarity and leading to fast partition into the aqueous environment from the NP core, they are indispensable for the pharmacological activity of attenuating β-catenin [20, 37]. The esterification of carboxyl functional groups with short or long aliphatic alcohols is one of the most widely used methods in prodrug strategy [38]. Therefore, five NCTD ester prodrugs were designed and synthesized, as indicated in Fig. 3A. In this study, the prodrugs NCTD-C4(C4), NCTD-C6(C6), NCTD-C8(C8), NCTD-C10(C10), and NCTD-C12(C12) were synthesized and characterized by TOF-MS, ^{1}H NMR ^{13}C NMR and Thin-layer chromatography (TLC) (Supplementary Fig. 4–18). The TOF-MS data provided molecular weight and formula information, while the NMR data helped verify the carbon backbone and hydrogen environments. TLC was conducted to assess the purity of the synthesized prodrugs. The results demonstrated clear, distinct spots for each compound, indicating the successful separation of the main components and supporting the purity of the samples. The TLC data for each prodrug are presented in Fig. S19. As predicted by Discovery Studio™ software (Fig. 3B), the lipophilicity (expressed as LogP) of NCTD ester prodrugs was substantially elevated compared to the NCTD lead compound. Among them, the logP values of prodrug NCTD-C8, NCTD-C10 and NCTD-C12 were very close to that of lomi, suggesting their extended-release profiles when encapsulated in NPs with lomi. Cumulatively, the physiochemical properties of the NCTD prodrugs have met our expectations for further investigation.

As PP2A is a key target of NCTD for downregulating β-catenin [18, 19], a further docking study was conducted to investigate the binding modes of the prodrugs to the PP2A protein (Protein Data Bank entry 2IE4). Based on the CDOCKER_ENERGY values, a higher value after docking indicates a more stable combination of the modified compound and the protein. The docking values of NCTD and its prodrugs with PP2A are shown in Fig. 3C. NCTD, as a PP2A inhibitor, has a docking value of 15.0532. Among the synthesized prodrugs, the docking values of C4, C6, and C8 are similar but significantly differ from that of NCTD, suggesting that their combination with PP2A may be unstable. In contrast, the docking values of C10 and C12 are close to that of NCTD, with the C12 value being higher, indicating that the combination of C12 and PP2A may be more stable. C12 adopted binding poses in the active site of the 2IE4 protein similar to those of the natural ligand NCTD (Supplementary Fig. 20, 21). The two carboxyl groups of NCTD can form hydrogen bonds (yellow line) with ARG214, ASN117 and HIS118, and the oxo bridge (red line) of the NCTD can form π-alkyl interactions with TYR127 (Fig. 3D). Similarly, the oxo bridge and two carbonyl groups in C12 can form hydrogen bonds (yellow line) with ARG214 and ASN117, and the cyclohexane ring in C12 can form hydrophobic interactions (cyan line) with TYR265, HIS59 and ARG214 (Fig. 3E). Thus, it can be concluded that C12 fits in the active sites of the PP2A protein similar to NCTD, indicating that the non-hydrolyzed NCTD derivatives also have the potential to downregulate β-catenin in a similar manner to NCTD.

Subsequently, we explored whether these NCTD-lipid prodrugs would achieve the desired pharmacological effects similar to NCTD. WB experiment was performed to identify the prodrugs' potential to suppress β-catenin in combination with lomi in TNBC cell lines. The WB analysis, conducted in triplicate, revealed that the combinations of "C8 + lomi" and "C12 + lomi" exhibited similar effects to "NCTD + lomi" in reducing both total and

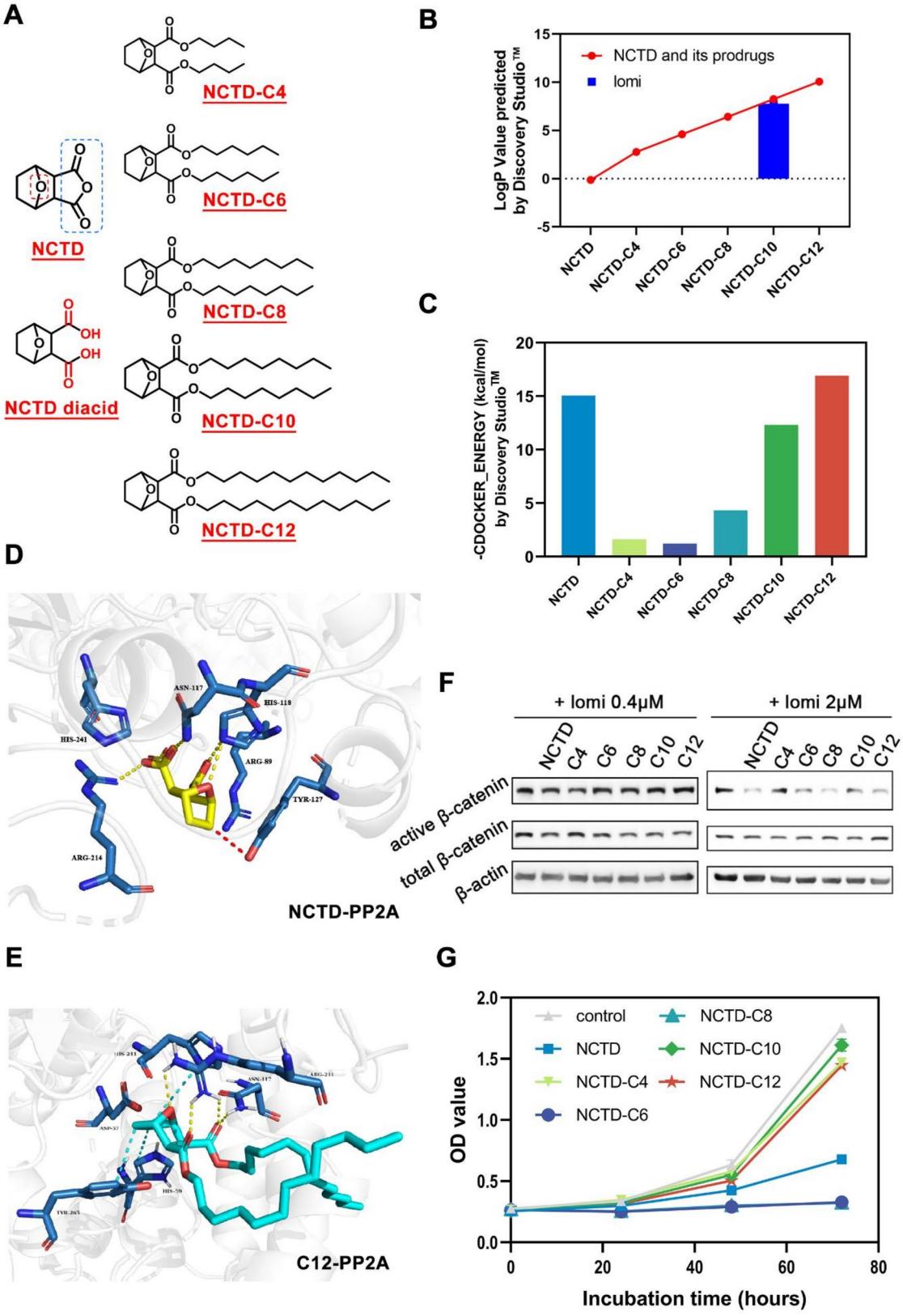

Fig. 3 (See legend on next page.)

(See figure on previous page.)

Fig. 3 Rational Design of NCTD-lipid Prodrugs for Co-Encapsulation with lomi.(**A**) Molecular structure of NCTD-lipid prodrugs. (**B**) LogP values of NCTD prodrugs predicted by Discovery Studio™ software, indicating hydrophobic properties. (**C**) Scoring of the docking of NCTD and its prodrug with PP2A molecules by Discovery Studio™ software. (**D**) Docking of NCTD (depicted in yellow) into the PP2A (PDB entry 2IE4). (**E**) Docking of NCTD-C12 (depicted in green) into the PP2A (PDB entry 2IE4). (**F**) Western blot analysis depicting active β-catenin and total β-catenin levels in TNBC 4T1 cells co-exposed to NCTD prodrugs (5 μM) and lomi (2 μM) for 24 h. (**G**) Non-specific cytotoxicity analysis of all five NCTD prodrugs via MTT assay. C6 and C8 demonstrated most pronounced effects on TNBC 4T1 cell growth. The data were presented as mean ± SD ($n = 6$)

active β-catenin levels. The quantitative data from three independent WB experiments were analyzed and presented in the accompanying column charts (Fig. 3F; Supplementary Fig. 22). These data consistently demonstrated that the NCTD modification did not affect its in vitro activity compared to unmodified NCTD.

Meanwhile, cytotoxicity was investigated to exclude non-specific effects against β-catenin (Fig. 3G). Compared to NCTD, prodrug C4, C10 and C12 at the dosage of 40 μM showed very mild effects against 4T1 cell proliferation, indicating that β-catenin downregulation by C12 was not due to non-specific cytotoxic effects. Considering lipophilicity, pharmacological activity, and non-specific cytotoxicity, C12 became the final candidate for NP loading.

The utilization of a prodrug strategy stands as a promising avenue for optimizing unfavorable physicochemical properties, augmenting stability, and achieving precise delivery without compromising activity. Cathepsins play integral roles in various processes linked to lysosomal functions, including protein degradation, protein and lipid metabolism, autophagy, antigen presentation, recycling of growth factor receptors, cellular stress signaling, and lysosome-mediated cell death [39]. We explored the degradation of released NCTD-C12 in a cathepsin B-sensitive manner via LC-MS/MS analysis. The hydrolysis experiment of NCTD-C12, conducted in the presence of cathepsin B, revealed the transformation of NCTD-C12 into NCTD after 72 h of incubation (Supplementary Fig. 23, 24). In vitro experiments demonstrated that the conversion rates of the prodrug C12 in a solution containing cathepsin B were 98.80% ± 0.59% (Fig. 4A). In vivo experiments (Fig. 4B) showed that in the extracellular environment, only 22.83% ± 21.56% of the prodrug C12 was converted to NCTD, indicating that C12 is more stable in the absence of cathepsin B in vivo. These results suggest that prodrug C12 exhibits high extracellular stability and can be converted to NCTD within cells, thereby prolonging the drug's therapeutic effect.

Engineering synergism-driving NP"C12 + lomi" formulation

In order to co-encapsulate NCTD-C12 with lomi in a single delivery system, they were mixed with lecithin and DSPE-PEG-RGD (synthesized from MAL-PEG-DSPE and RGD-SH via Michael addition reaction [24]) to form nanoparticles through self-assembly using high-pressure homogenization method. The highly lipophilic NCTD-C12 and lomi formed the hydrophobic core, while the phospholipids of DSPE-PEG-RGD stabilized the nanoparticles via the principle of similar phase solubilization. The hydrophilic terminus of PEG, which is connected to the RGD peptide, enabled tumor-targeting, leading to the successful formation of the NP"C12 + lomi". The physical properties of these NPs were subsequently characterized. The encapsulation efficiencies (EE%) of C12 and lomi within NP"C12 + lomi" were determined to be 98.22 ± 3.20% and 86.77 ± 6.34%, respectively. At a concentration of 1 mg mL^{-1} of C12, the size of the loaded NPs was approximately 100–130 nm, with an average diameter of 127.7 ± 1.8 nm, while the blank nanoparticles had a smaller size of 80.2 ± 2.3 nm. The increase in particle size for the loaded NP suggests that drug encapsulation resulted in a larger nanoparticle, which is commonly observed when drug molecules are incorporated. Furthermore, we repeated the Transmission Electron Microscopy (TEM) imaging to obtain representative images with more nanoparticles (Supplementary Fig. 25, 26). The average size of the loaded NPs was 76.2 ± 19.5 nm, while that of the blank nanoparticles was 67.3 ± 25.8 nm. Although the absolute sizes measured by TEM were smaller than those obtained by Dynamic Light Scattering (DLS), this discrepancy is expected due to differences in the measurement principles. Nevertheless, both methods revealed a clear size increase upon drug loading. Furthermore, the size distribution observed from TEM is consistent with the PDI values measured by DLS (0.371 for NP"C12 + lomi" and 0.331 for NP blank), supporting the relatively narrow size distribution and acceptable homogeneity of the nanoparticles. The Zeta potential of the NP"C12 + lomi" was − 35.1 ± 2.2 mV, significantly more negative than that of the NP blank, which exhibited a Zeta potential of -15.1 ± 2.0 mV. This notable difference in Zeta potential indicates that the drug loading not only increased the particle size but also enhanced the stability of the NPs due to the increased negative surface charge (Fig. 4C, D; Supplementary Fig. 27, 28). The particle size of NP"C12 + lomi" in PBS and RPMI-1640 was maintained at approximately 100 nm over 15 days, suggesting good stability under normal physiological condition (Fig. 4E). The DSC analysis of NP"C12 + lomi" shows that the original crystal characteristic peak of C12 and the peak of lomi disappear. This suggests that the drug may have transformed into an amorphous state within the nanoparticles, indicating successful

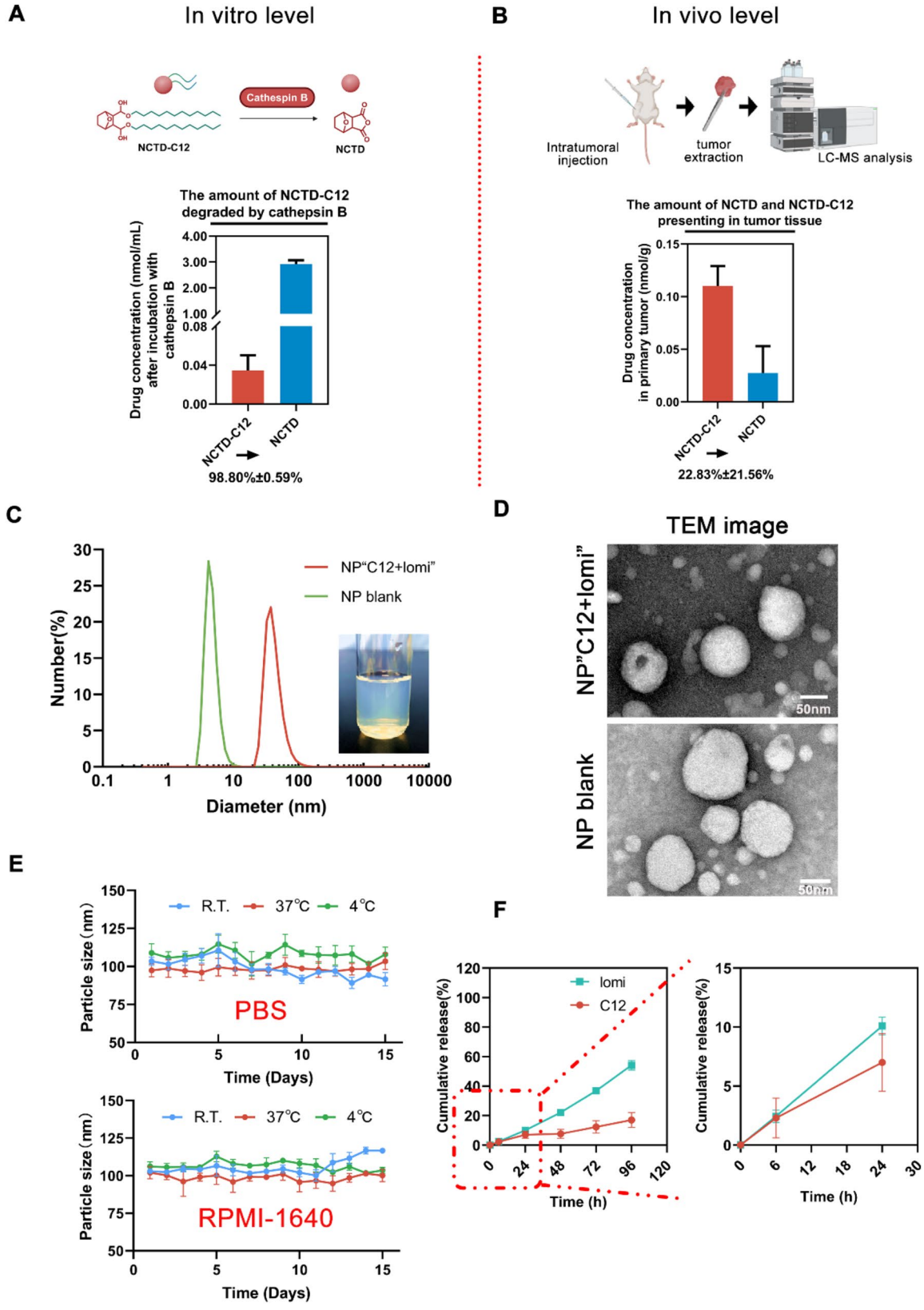

Fig. 4 (See legend on next page.)

(See figure on previous page.)

Fig. 4 Fabrication and characterization of NPs co-loaded with lomi and C12.(**A**) In vitro analysis of cathepsin B-responsive prodrug NCTD-C12. In the presence of 10 unit mL^{-1} cathepsin B, 1 mg mL^{-1} NCTD-C12 was incubated in sodium acetate solution (pH 5.0) with 10 U mL^{-1} cathepsin B for 72 hours. The final concentrations of NCTD and NCTD-C12 were determined by LC-MS/MS, the transition pairs of NCTD and NCTD-C12 were *m/z* 168.94→67 and 523.4→123, respectively. (**B**) In vivo analysis of cathepsin B-responsive NCTD-C12. C12 was administered via intratumoral injection at a dosage of 10 mg kg^{-1} when the tumor size reached ≈ 100 mm^3. After 72 h, tumors were extracted, homogenized, and analyzed further by LC-MS/MS. (**C**) Determination of NP"C12 + lomi" size and NP blank using DLS method and the appearance of the NP"C12 + lomi". (**D**) Representative TEM image showcasing NP"C12 + lomi" and NP blank. Scale bar, 50 nm. (**E**) Stability of NP"C12 + lomi" under various conditions. The NP were tested in cell culture fluids (RPMI-1640) and PBS at different temperatures (room temperature, 4 °C, and 37 °C). The particle size was measured over time to assess the stability of the NP under these conditions. (**F**) In vitro release profiles of lomi, and C12 from NP"C12 + lomi" in pH 7.4 PBS with 1% Tween 20

drug encapsulation (Supplementary Fig. 29). TLC analysis showed that the NP blank exhibited only a spot corresponding to the lipid component, while the C12 and lomi NP showed spots corresponding to their respective drug components. The NP"C12 + lomi" displayed two spots, representing the C12 and the lomi, indicating the successful co-encapsulation of both in the nanoparticles (Supplementary Fig. 30). We further investigated the intracellular localization of Cy5-labeled nanoparticles (Supplementary Fig. 31). The results showed significant co-localization of the nanoparticles with the endoplasmic reticulum, supporting their potential as effective drug delivery carriers capable of functioning in specific cellular regions. Collectively, these findings affirm the successful co-entrapment of C12 and lomi, leveraging their respective lipophilic properties.

The underlying design concept of the synergism-driving NPs underscores the importance of an extended-release profile for the simultaneous colocalization of multiple payloads at specific sites [40]. To this end, a release-profile study was conducted. As depicted in Fig. 4F, approximately 10% of C12 or lomi was released from NP"C12 + lomi" after 24 h of incubation in PBS (1% Tween 20) at pH 7.4. Both C12 and lomi exhibited similar sustained-release patterns (Supplementary Fig. 32, 33). In stark contrast, the parent compound NCTD exhibited rapid release from the NP"C12 + lomi", with nearly 100% of the drug released within the first 24 h. The data for NP"C12 + lomi" best fit the Korsmeyer-Peppas model. For the C12, the release followed the Korsmeyer-Peppas model (R^2=0.962), with an exponent value of $n = 0.65$, indicating anomalous diffusion, where both diffusion and dissolution contributed to the release. In contrast, lomi followed the Korsmeyer-Peppas model (R^2=0.993), with an exponent value of $n = 1.02$, suggesting erosion-controlled release. These findings support the hypothesis that NP"C12 + lomi" can effectively facilitate small molecule colocalization in complex physiological environments, which is crucial for achieving pharmacological synergism. Additionally, we found that the conversion of C12 to NCTD in NPs in the presence of cathepsin B in vitro was 87.52%±5.17% (Supplementary Fig. 34), which differed little from the prodrug C12 conversion efficiency (98.80%±0.59%) mentioned above. The results indicated that the NPs did not affect the efficiency of the conversion of C12 to NCTD. To confirm the physical interaction and co-localization of the molecules, FRET efficiency was monitored over 8 h. As shown in Fig. S35, the FRET efficiency remained stable from 46.91% (0 min) to 45.05% (8 h), with only a minor decrease of 1.86% over the observation period. These results indicate that the molecular interaction remains stable over time, suggesting a persistent close proximity between the donor and acceptor molecules. The minimal fluctuation in FRET efficiency further suggests that no significant dissociation or structural reorganization occurred within the timeframe of the experiment.

Enhanced in vitro CCL4 expression mediated by synergistic NP"C12 + lomi"

Inappropriate activation of the Wnt pathway has been shown to drive cell proliferation [30], and β-catenin translocation into the nucleus can result in the activation of multiple genes, including cyclin D1 and cMyc, whose transcription triggers cell proliferation advancement. In order to better demonstrate the advantages of the C12, we conducted a comparative study of nanoparticles co-loaded with various prodrugs and lomi. WB experiments showed that the NP"C12 + lomi" significantly reduced the expression of both total and active β-catenin (Supplementary Fig. 36). Additionally, the CCL4 and CD24/CD44 expression levels in the NP"C12 + lomi" group were significantly higher compared to the other groups (Supplementary Fig. 37, 38). This suggests that the NP"C12 + lomi" formulation not only impacts the β-catenin signaling pathway but may also promote a more favorable immune microenvironment, potentially enhancing the therapeutic effects by altering the stem-like characteristics of the tumor cells. The increased CD24/CD44 ratio indicates a reduction in the cancer stem cell population, which could contribute to the improved anti-tumor activity observed with this formulation. The drug-loaded NPs with varying NCTD prodrugs demonstrated a potent dose-dependent suppression of 3D soft agar colony formation in 4T1 cells (Supplementary Fig. 39). Notably, NPs conjugated with lomi and longer carbon chains (NP"C10 + lomi" and NP"C12 + lomi") exhibited near-complete inhibition of colony formation, which was significantly lower than both the control group and short-chain counterparts. This trend was further

supported by spheroid formation analysis (Supplementary Fig. 40). Treatment with NP"C12 + lomi" resulted in both the smallest spheroid size and the fewest spheroids, outperforming all other groups. The results of the above experiment provide strong evidence that increased hydrophobicity and enhanced drug retention from longer-chain NPs contribute to improved anti-tumor effects.

An MTT study (Fig. 5A) was performed to analyze the proliferation of 4T1 cells exposed to NP"C12 + lomi" and free"C12 + lomi". NP"C12 + lomi" inhibited 4T1 cell growth more efficiently than free"C12 + lomi" at lower dosages (C12 + lomi: 2.5 μM + 1 μM, 5 μM + 2 μM) due to the greater suppression of β-catenin. However, as the dosages increased, the distinction between the two treatments disappeared, which may be attributed to the cytotoxic effects overwhelming the synergistic attenuation of β-catenin. To further assess the synergistic effect of the NP"C12 + lomi" combination, the combination index (CI) was calculated using the formula CI = Cl/IC50 + Cn/IC50, where Cl and Cn represent the concentrations of C12 and lomi. The CI value for NP"C12 + lomi" was found to be 0.11, suggesting a synergistic effect between the two drugs at the tested concentrations. In addition, the hemolysis assay results showed that the positive control group (pure water) caused significant red blood cell lysis, while the negative control group (physiological saline) did not exhibit any hemolysis. The different nanoparticle treatment groups (NP blank, lomi NP, C12 NP, NP"C12 + lomi") showed similar results to the negative control group, with no significant red blood cell lysis, indicating good biocompatibility of these nanoparticles in blood (Supplementary Fig. 41). We performed a cell migration assay with the same groups at four time points: 0 h, 6 h, 24 h, and 48 h. The final results demonstrated that NP"C12 + lomi" curtailed the migration of TNBC 4T1 cells (Supplementary Fig. 42).

The in vitro cell-based assays explored whether the synergistic NP could efficiently promote CCL4 expression. It was assumed that the integrated NP would achieve the synergism ("high expression") of "C12 + lomi" more efficiently than the free drugs, which would exhibit reduced efficacy due to NP disassociation ("low expression") in physiological environments (Fig. 5B). To test this, 4T1 cells were continuously treated with saline, NP"C12 + lomi", free"C12 + lomi", and a blank NP vehicle over eight generations. As shown in Fig. 5C, qPCR analysis detected an upward trend in CCL4 expression levels after stimulating 8th generation 4T1 cells with the synergistic NP. Compared to the control group, NP"C12 + lomi" successfully boosted CCL4 expression 10-folds in 8th passage 4T1 cells, whereas the free"C12 + lomi" combination did not alter CCL4 expression. This indicates that long-term treatment with the synergistic NP can induce CCL4 expression in cancer cells.

To determine whether the observed changes were induced by β-catenin suppression, several β-catenin phenotypic studies were performed. As indicated by the WB results in 4T1 cells of 1st culture passage (Fig. 5D; Supplementary Fig. 43), NP"C12 + lomi" attenuated both active and total β-catenin expression levels more effectively than the free"C12 + lomi" treatment, suggesting that the synergistic NP could more efficiently suppress β-catenin by leveraging small-molecule co-localization. As a nuclear-cytoplasmic shuttling protein, the nuclear localization of β-catenin indicates its activation to increase target gene expression [21]. β-catenin immunofluorescence (IF) staining showed that β-catenin is mainly localized in nucleus in 4T1 cells, as evidenced by the merged pinkish color from β-catenin IF staining (red) and nuclear DNA (deoxyribonucleic acid) DAPI fluorescent staining (blue) (Fig. 5E). In line with the WB analysis results showing diminished β-catenin level in 4T1 cells, very little and weak pinkish color was observed in cells exposed to NP"C12 + lomi" or free"C12 + lomi" for 48 h, indicating significantly less β-catenin nuclear localization. Notably, compared to the free"C12 + lomi (5 μM, 2 μM)" group, less β-catenin remained in the cytosol of 4T1 cells in the NP"C12 + lomi (5 μM, 2 μM)" groups.

CSCs are generally enriched in nonattached sphere cultures, reflecting their anchorage-independent self-renewal capacity. To examine this ability, 4T1 cells were cultured under anchorage-independent conditions in serum-free RMPI1640 medium in the absence or presence of C12 and lomi at dosages of 5 μM and 2 μM, respectively. The presence of NP"C12 + lomi" most effectively inhibited sphere formation, as evidenced by the smaller sphere size in Fig. 5F. Fewer spheres also highlighted the potential of the synergistic NP to impair the self-renewal property of CSCs, which is usually maintained by activated Wnt/β-catenin signaling (Fig. 5G). These results were consistent with the qPCR results, suggesting that the synergistic NP likely induced CCL4 expression via β-catenin suppression. Therefore, by leveraging synergism, NP encapsulation safely confers modulator-like functions to the "C12 + lomi" combination and has a great chance to avoid their "on target, off tumor" toxicities in vivo.

Immunotherapy responses arising from the treatment of synergistic NP

Having confirmed the in vitro potency of the synergistic NP, we next sought to identify its in vivo potency to stimulate immune system. The results of organ distribution of Cy7.5-labeled NPs were showed as Fig. S44. In the NP"C12 + lomi" group, prominent fluorescence signals were observed in both the liver and tumor tissues. Notably, the fluorescence intensity in the tumor region was significantly higher than in other areas, indicating that

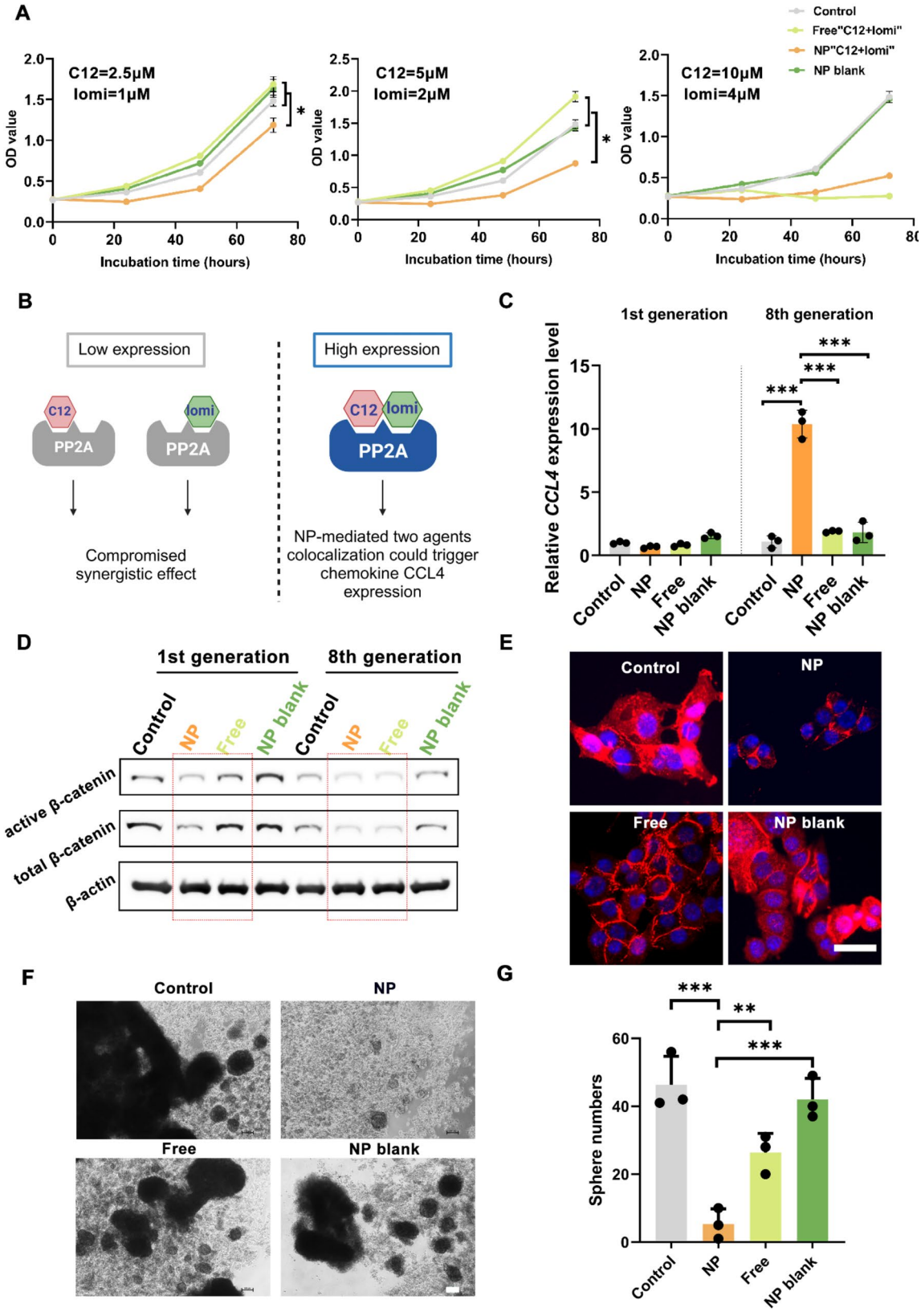

Fig. 5 (See legend on next page.)

(See figure on previous page.)

Fig. 5 In Vitro Assessment of NP"C12 + lomi" for β-catenin deactivation in TNBC 4T1 Cells. (**A**) Growth curves of 4T1 cells. Cell growth was monitored through optical density (OD) values ($n = 6$, $^{*}P < 0.05$). 4T1 cells were treated with the indicated agents for 0, 24, 48, and 72 h. (**B**) Schematic illustration outlining the synergistic role of NP. This diagram outlines NP synergistic role in toggling the expression of CCL4 high or low. (**C**) Quantitative PCR analysis of CCL4 expression. 4T1 cells were subjected to various treatments, including saline, NP"C12 + lomi", free"C12 + lomi", or NP blank. Each treatment group underwent continuous culture over 8 passages, with a 48-hour treatment duration in each passage ($n = 3$, $^{***}P < 0.001$). (**D**) Western blot analysis of active β-catenin and total β-catenin levels. 4T1 cells from the 1st and 8th generations were analyzed for active β-catenin and total β-catenin levels. (**E**) Representative IF images of β-catenin. 4T1 Cells were exposed to saline, NP"C12 + lomi", free"C12 + lomi", or NP blank for 48 h and then fixed by 4% paraformaldehyde for further IF staining. Scale bar, 50 μm. (**F**) Sphere formation assay. This assay demonstrates reduced sphere-forming activity in 4T1 cells with the indicated treatments. The spheres were cultured in a 10-day cycle. Scale bar, 100 μm. (**G**) Cells were photographed and counted. The graph represents the mean ± SD ($n = 3$). $^{**}P < 0.01$; $^{***}P < 0.001$

the nanoparticles effectively accumulated in the tumor. In contrast, free Cy7.5 primarily accumulated in the liver, with relatively weak fluorescence signals observed in the tumor region. This differential distribution suggests that the nanoparticles, through specific biodistribution mechanisms, are able to target and accumulate in the tumor.

TNBC generally presents as a "cold tumor" with limited effector T cells infiltration, largely attributed to the loss of CCL4 expression in TME [1]. Therefore, we aimed to investigate whether normalizing CCL4 by the synergistic NP could restore immune status and boost immunotherapy for TNBC. A murine TNBC model using 4T1 cells was established to assess this hypothesis. Murine 4T1 cells were orthotopically inoculated into the fourth fat pad of female Balb/c mice. The formulations were administered intravenously (*i.v.*) twice per week for three weeks once the tumors grew to approximately 100 mm^3. As shown in Fig. 6A, fluorescence-activated cell sorting (FACS) analysis of the 4T1 primary tumors revealed increased immune cell infiltration, particularly $CD45^+CD3^+CD8^+$T cells. Additionally, more $CD45^+CD11b^+CD11C^+Gr1^-F4/80^-$ dendritic cells (DCs) were infiltrated in the tumor, which typically promote T cell migration to the TME. Thus, the activated $CD8^+$ cytotoxic T-cells returned to the primary tumor site with the help of NP"C12 + lomi", likely due to the high expression of CCL4. Notably, these therapeutic outcomes were achieved without significant changes in animal body weight, indicating the absence of systemic toxicity (Supplementary Fig. 45).

The accumulation of gene mutations blunts antitumor immunity by excluding $CD8^+$ T cells from tumors in a Wnt/β-catenin signaling-dependent manner [41]. Consistent with this report, we found fewer active β-catenin positive cells in 4T1 primary tumors, as evidenced by the merged pinkish color from β-catenin IF staining (red) and nuclear DNA DAPI fluorescent staining (blue) (Fig. 6B).

Research on $CD8^+$ T cell-dependent antitumor immunity has traditionally emphasized its role within primary tumors. Despite limited impact on primary tumor growth (Supplementary Fig. 46), the treatment group receiving synergistic NPs demonstrated elevated levels of $CD8^+$ T cells in the bloodstream (Fig. 6C), prompting us to further investigate the potential antitumor activity of NP"C12 + lomi". The increase in cytotoxic $CD8^+$ T cell population in blood suggested NP"C12 + lomi" potential against metastasis.

To further elucidate the potential mechanism of the NP"C12 + lomi" in anti-tumor therapy, we investigated the therapeutic role of either C12 or lomi nanoparticles alone, or NP"C12 + lomi". We observed the NP"C12 + lomi" significantly increased the number of cytotoxic IFN-γ^+ $CD8^+$ T cells, granzyme B^+ $CD8^+$ T cells and cytotoxic IFN-γ^+ $CD4^+$ T cells in both the tumor tissues and lymph nodes (Supplementary Fig. 47). In addition, the tumor growth curves (Supplementary Fig. 48) showed that the co-loaded nanoparticles significantly suppressed tumor growth compared to the control and single drug treatments. This suggests that the combined therapy of C12 and lomi may promote a more robust activation of $CD8^+$ T cells, potentially enhancing their anti-tumor effects. From the images of the H&E-stained tissue sections (Supplementary Fig. 49), no obvious pathological variation in all groups was observed, indicating that the NP"C12 + lomi" therapy did not induce noticeable tissue toxicity or injury in the studied organs.

NP-Mediated colocalization of small molecules enhances mitigation of lung metastasis in a post-surgery TNBC model

In the landscape of cancer treatments, surgery plays a fundamental role. However, it often faces the risk of incomplete resection and susceptibility to recurrence. To address this issue, we aimed to delineate the primary tumor's anatomical boundaries and ascertain the post-surgical potential of synergistic NPs in preventing tumor relapse and suppressing metastatic tendencies. To establish an orthotopic breast tumor model characterized by spontaneous metastases, luciferase-expressing 4T1 tumor cells (4T1-Luc) were inoculated into the mammary fat pad of BALB/c mice. When the tumor volume in the mice reached approximately 500 mm^3, simulating post-surgery residual micro-tumor conditions, we executed tumor resection. As illustrated in Fig. 7A, this surgical procedure was followed by subsequent recovery. The mice were then stratified into distinct subgroups, each receiving weekly administration of either

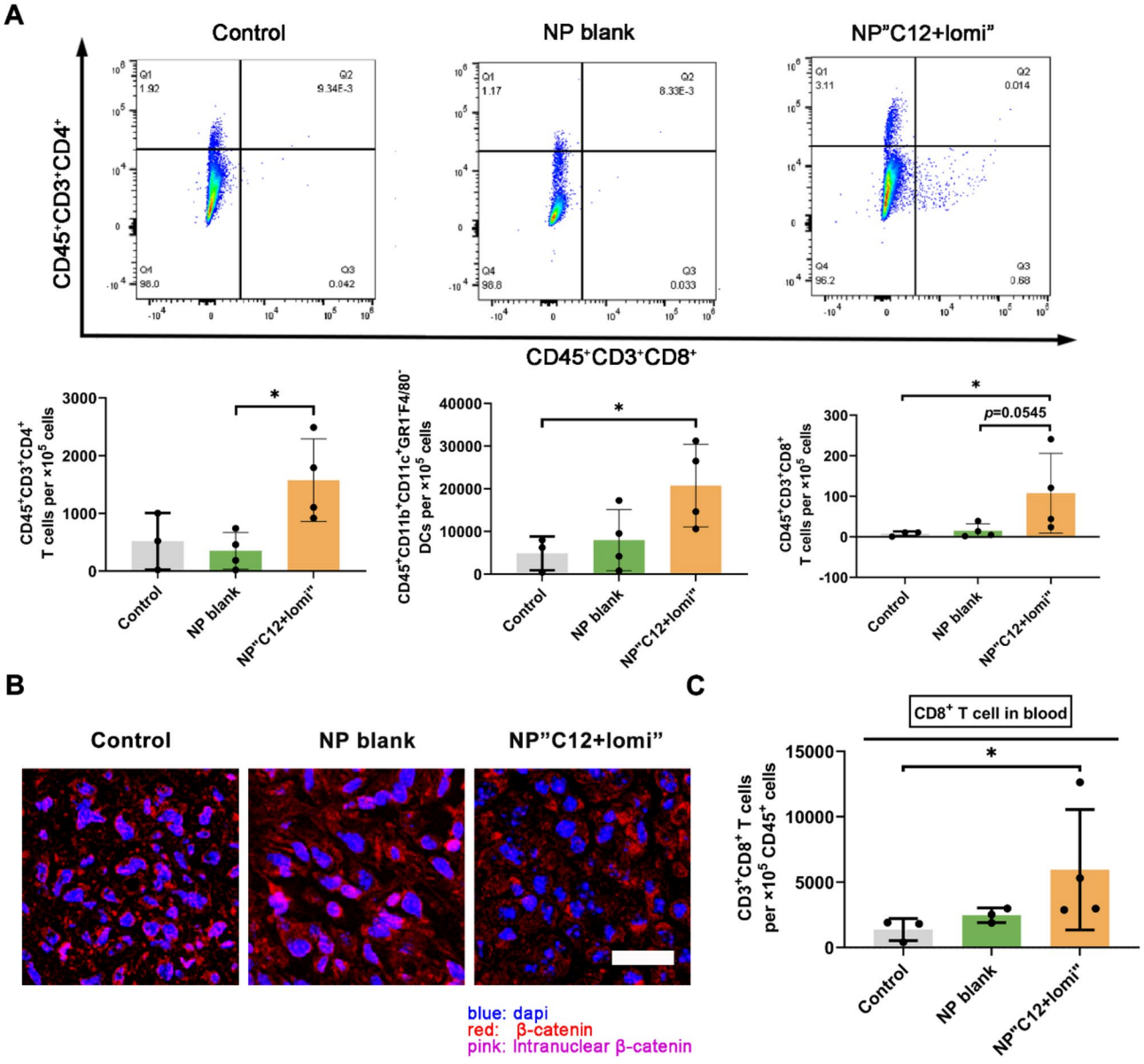

Fig. 6 NP"C12 + lomi" enhancing cytotoxic $CD8^+$T cells and its potential for combinatorial use with ICI agent. (**A**) Flow cytometry analysis of immune cell populations in 4T1 primary tumors treated with NP"C12 + lomi". Flow cytometry was employed to assess immune cell populations, including $CD45^+CD1$ $1b^+CD11C^+Gr1^-F4/80^-$ DC, $CD45^+CD3^+CD4^+$ T cells, and $CD45^+CD3^+CD8^+$ T cells, within 4T1 primary tumors treated with NP"C12 + lomi". Mice bearing 4T1 tumors were euthanized on day 29 post-inoculation, and primary tumors were harvested for analysis, using the gating method detailed in Supplementary Fig. 50. Data with significance were denoted as $*P < 0.05$. (**B**) IF staining of β-catenin in 4T1 primary tumors. IF staining was conducted to visualize active β-catenin levels and cellular localization within 4T1 primary tumors. Fluorescent signals depict the relative levels of active β-catenin. NP"C12 + lomi" makes more cytosolic β-catenin undergo the destruction process into the proteasome and less β-catenin were transcribed to suppress CCL4 expression. Scale bar, 25 μm. (**C**) Comparison of final primary tumor weights and cytotoxic $CD8^+$ T cells in blood among indicated groups. Despite limited impact on primary tumor growth, the increase in cytotoxic $CD8^+$ T cell population in blood suggested NP"C12 + lomi" potential against metastasis

free"C12 + lomi" or NP"C12 + lomi" with a 7-day interval following tumor resection. We comprehensively evaluated postoperative recurrence and metastasis in TNBC, involving sequential luminescence imaging at relevant junctures or thoracic areas (Fig. 7B). Analytical insights gathered on day 26 and day 47 post-tumor dissection distinctly demonstrated the superior inhibitory efficacy of synergistic NP against tumor metastasis.

Our study highlights the potential of nanoparticle-based treatment as a novel approach to address these challenges. The primary aim of these interventions was to enhance murine survival rates. To this end, a comprehensive survival analysis was conducted, involving meticulous observation of the survival duration of mice over a period of 76 days. In this experiment, day 0 is defined as the day of tumor inoculation. This translated

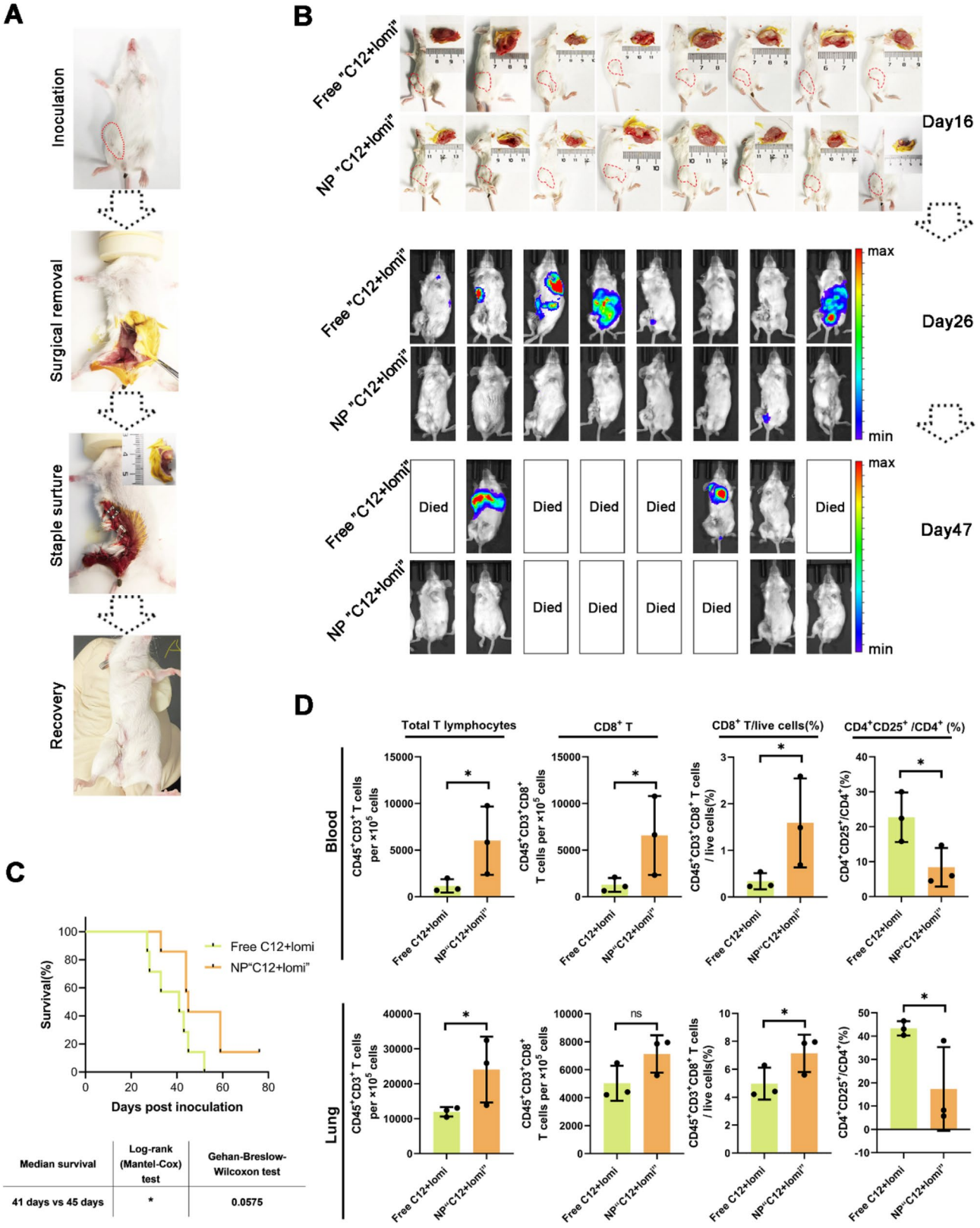

Fig. 7 Antimetastatic efficacy of NP"C12 + lomi" in the 4T1 post-surgery model due to the colocalization of small molecules. (**A**) A schematic summary of how the 4T1 post-surgery model was established. (**B**) Metastases progression was monitored quantitatively in the free"C12 + lomi" and NP"C12 + lomi"-treated groups at day 26 and day 47 after inoculation using biophotonic imaging analysis. (**C**) Survival analysis of treated mice ($n = 7$). (**D**) Quantification of metastases-infiltrating lymphocytes in blood and lung from BALB/c mice ($n = 3$). *$P < 0.05$

to a substantial improvement in survival rates, as depicted in Fig. 7C. The median survival times for the NP"C12 + lomi" and the free"C12 + lomi" groups were 59 days and 43 days, respectively. The prolongation of the survival period may be attributed to the anti-lung metastasis efficacy of the NP treatment. Additionally, we recorded the longitudinal alteration in body weight, as depicted in Fig. S51. The body weights of mice in each specific treatment group were tracked at 7-day intervals. Crucially, over the entire treatment duration, the body weight of mice in both experimental groups remained remarkably stable, emphasizing the safety profile of the developed synergistic NP throughout the therapeutic regimen. In comparison to traditional postoperative chemotherapy, which often comes with significant side effects and variable efficacy in TNBC, our NP treatment demonstrated several advantages. The targeted delivery of drugs via nanoparticles allows for more precise drug delivery to the tumor site, reducing damage to healthy tissues and minimizing side effects [42]. Additionally, the ability to co-deliver multiple therapeutic agents within a single nanoparticle system enhances the synergistic effects of the drugs, potentially overcoming limitations seen with free drug administration [43].

The distinct therapeutic outcomes of "C12 + lomi" with or without NP suggest an involvement of the immune system. Systemic treatment with STING agonists in mice has been reported to eliminate dormant metastasis and prevent spontaneous outbreaks in a T cell-dependent manner [44]. Thus, we investigated whether the inhibition of tumor metastasis by synergistic NP relies on a T cell-dependent mechanism. FACS analyses of mice lungs and blood revealed increased expression levels of $CD8^+$ T cells in the lungs of NP-treated mice. Significantly increased $CD45^+CD3^+$ T cell infiltration was observed in tumors treated with NP"C12 + lomi". The $CD8^+$ cell populations were also elevated, while the percentage of $CD4^+CD25^+$ T regulatory cells decreased (Fig. 7D). Elevated levels of serum CCL4 have been reported to improved disease-free survival [31]. In line with this, the administration of NPs facilitated prolonged inhibition of 4T1 metastasis without inducing significant toxicity. Mechanistically, we observed robust infiltration of immune effector cells, notably $CD8^+$ T cells, into lung tissues and blood. Therefore, the physical co-localization of the two drugs appears to achieve a better therapeutic effect compared to the free drug. Our findings suggest that nanosystems could serve as ideal dual-drug delivery systems, enhancing the synergistic effects between drugs. Subsequent investigations will integrate NP with other immunotherapeutic approaches to assess its synergistic efficacy in suppressing metastatic progression.

Synergistic antitumor and antimetastatic effects of application NP"C12 + lomi" with BMS1016

BMS company once designed a series of small-molecule PD-1/PD-L1 interaction inhibitors, such as BMS1016, which significantly increased anti-PD-1/PD-L1 activity [45, 46]. We previously tested the efficacy of BMS1016 combined with a β-catenin suppressor [46] and observed a trend of decreased CCL4 expression was in long-term experiments with the BMS1016, while NP"C12 + lomi" treatment resulted in increased CCL4 expression (Supplementary Fig. 52). Reportedly, combined treatment with PD-1 blockade and Wnt/β-catenin signaling inhibitors induces better antitumor immunity than either treatment alone [41]. Thus, we propose a mechanism-oriented combination therapy where an ICI agent is combined with NP"C12 + lomi". Similar to our previous study [46], BMS1016 was chosen as the ICI agent due to its intrinsic low immunogenicity as a small molecule.

In both 4T1 and E0771 cells, the combinatorial use of NP"C12 + lomi" and BMS1016 significantly elevated the secretion of CCL4 in a synergistical manner (Fig. 8A). Additionally, β-catenin activation can elevate PD-L1 expression in tumor cells by binding the β-catenin/TCF/LEF complex to the *CD274* gene promoter region, leading to immune evasion in glioblastoma [47]. In the present study, the combinatorial use of NP"C12 + lomi" and BMS1016 effectively diminished these unfavorable outcomes in 4th passage 4T1 cells. The WB analysis, revealed that the NP"C12 + lomi" + BMS1016 combination treatment significantly reduced PD-L1 expression than the NP"C12 + lomi" or BMS1016. The quantitative results are presented in the accompanying column chart (Fig. 8B, Supplementary Fig. 53). In a tumor cell-T cell co-culture system, the BMS1016 + NP"C12 + lomi" combination demonstrated synergistic immunostimulatory effects, with significantly enhanced T cell proliferation compared to individual treatments (Supplementary Fig. 54), indicating enhanced T cell proliferation and potential immunostimulatory effects of the combined regimen. Taken together, these in vitro results strongly suggest the substantial potential of combining NP"C12 + lomi" with ICI agents and promote further in vivo studies.

We tested the antitumor efficacy of BMS1016 combined with NP"C12 + lomi" in a 4T1 tumor model following the schedule in Supplementary Fig. 55. Small molecules are favored for their better oral availability compared to biologics. Thus, we included an oral administration group in the in vivo study. When tumor volumes reached approximately 100 mm^3, groups of five mice received the following treatments: (1)saline, (2)BMS1016 (1 mg kg^{-1}, intraperitoneally, *i.p.*) + oral NP"C12 + lomi" (20 mg kg^{-1}, 10 mg kg^{-1})", (3)BMS1016 (1 mg kg^{-1}, *i.p.*) + *i.v.* NP"C12 + lomi" (20 mg kg^{-1}, 10 mg kg^{-1})", (4)BMS1016 (1 mg kg^{-1}, *i.p.*) + *i.v.* NP vehicle

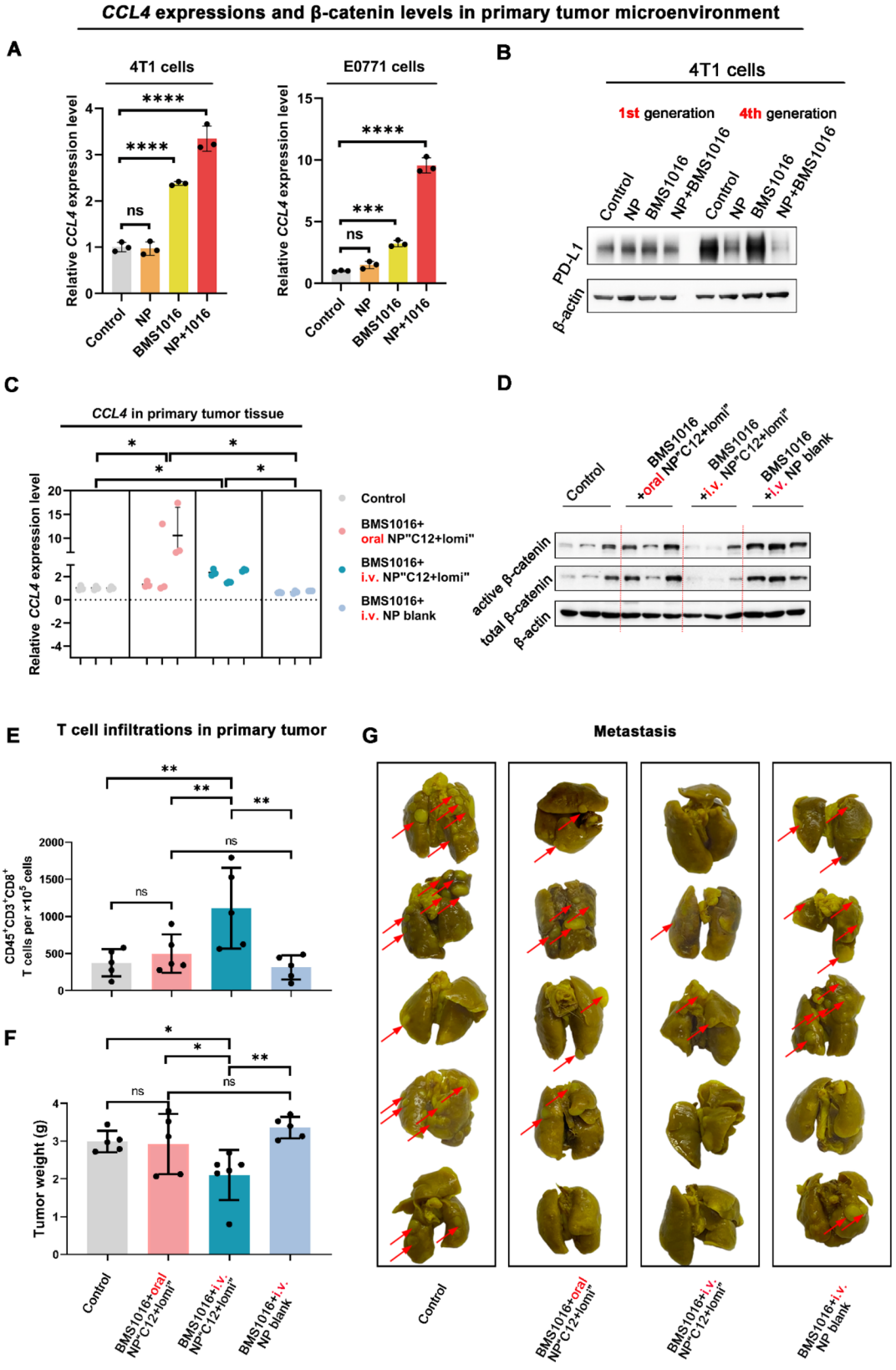

Fig. 8 (See legend on next page.)

(See figure on previous page.)

Fig. 8 Antitumor efficacy of the combinatorial use of BMS1016 and NP"C12 + lomi" in the 4T1 Orthotopic TNBC Model. (**A**) Enhancement of CCL4 expression in TNBC 4T1 and E0771 cells with combinatorial use. Quantitative PCR analysis demonstrated elevated CCL4 expression in 4T1 and E0771 cells with the combinatorial use of BMS1016 and NP"C12 + lomi". (**B**) Reduction of PD-L1 expression in 4T1 cells after long-term combinatorial treatments. WB analysis indicated diminished PD-L1 expression in 4T1 cells following prolonged combinatorial treatments with BMS1016 and NP"C12 + lomi". (**C**) qPCR analysis of CCL4 levels in 4T1 primary tumors using GAPDH as an internal control ($n = 3$, $^{*}P < 0.05$). (**D**) WB analysis of 4T1 primary tumors. WB analysis was performed for a panel of Wnt signaling markers, active and total β-catenin with β-actin serving as a loading control. Less β-catenin due to NP"C12 + lomi" treatment was transcribed to suppress CCL4 expression. (**E**) Flow cytometry analysis of $CD45^{+}CD3^{+}CD8^{+}$ T cell populations in primary tumors. Flow cytometry quantified $CD45^{+}CD3^{+}CD8^{+}$ T cell populations in primary tumors collected on day 36 ($n = 5$, $^{**}P < 0.01$). (**F**) Mean primary tumor weights for each treatment group ($n = 5$; ns, not significant; $^{*}P < 0.05$; $^{**}P < 0.01$). (**G**) Ex vivo images of lungs with metastatic nodules observed after 72-hour immersion in Bouin's fixative. Tumor metastasis is indicated by the red arrow

every 3 days for a total of 10 (NP"C12 + lomi") or 4 (BMS1016) administrations. After 3 weeks of treatment, CCL4 levels in tumor burden were quantified by qPCR (Fig. 8C). Both oral and *i.v.* NP"C12 + lomi" combined with BMS1016 caused appreciable changes compared to the control mice. We further performed immunoblot analysis of tumor lysates for Wnt markers (total and active β-catenin) to investigate the association between CCL4 expression and β-catenin attenuation in the animals treated with BMS1016 + NP"C12 + lomi". In agreement with changes in CCL4 expression, we observed appreciable change in total and active β-catenin after BMS1016 + *i.v.* NP"C12 + lomi" treatments. However, tumors treated with BMS1016 + oral NP"C12 + lomi" did not show the same deactivation, as indicated by the weaker bands, this discrepancy was also reflected in the corresponding quantitative analysis (Fig. 8D; Supplementary Fig. 56).

The moderate efficacy could be explained by the different pharmacokinetic profiles of the oral and *i.v.* administration routes, evidenced by the lower plasma concentrations in Supplementary Fig. 57. Specifically, *i.v.* NP"C12 + lomi" administered at the same dosage of 20 mg kg^{-1} (C12) and 10 mg kg^{-1} (lomi) resulted in plasma concentrations of C12 and lomi that were over 100-fold higher than those in the oral NP"C12 + lomi" group. This plasma concentration-time profiles upon *i.v.* administration to rats disclosed the long-circulation feature of *i.v.* NP. However, even when NP"C12 + lomi" reaches the gastrointestinal tract, it still faces barriers regarding stability and absorption.

In line with the results of CCL4 expression levels, the quantification of $CD45^{+}CD3^{+}CD8^{+}$ T cell number in primary tumor tissue demonstrated an increase from two treatment modalities: BMS1016 + oral NP"C12 + lomi" and BMS1016 + *i.v.* NP"C12 + lomi" (Fig. 8E). The more robust contribution came from the BMS1016 + *i.v.* NP"C12 + lomi" group, which showed a nearly 2-fold increase in $CD45^{+}CD3^{+}CD8^{+}$ T cells compared to the control group. Moreover, BMS1016 + *i.v.* NP"C12 + lomi" had the most potent effect on reducing 4T1 primary tumor growth, whereas BMS1016 + NP vehicle had little effect (Fig. 8F). These findings indicate that the combination of intravenously administered NP"C12 + lomi" and immune checkpoint therapy exhibits a pronounced inhibitory effect on orthotopic tumors.

Inappropriate activation of the Wnt pathway has been shown to drive cell proliferation and tumor formation [30]. With most solid-tumor cancers, the biggest danger is not the tumor itself but its ability to metastasize. Metastasis is the leading cause of cancer death [48] and has an inverse association with $CD8^{+}$ T cells [49]. Activation of the Wnt/β-catenin signaling pathway is observed in various tumor cells and results in metastasis. Significantly, BMS1016 + *i.v.* NP"C12 + lomi" also showed the most potent anti-metastasis efficacy, evidenced by the reduced lung metastatic nodules in the 4T1 tumor model (Fig. 8G). In contrast, BMS1016 + NP vehicle barely had $CD8^{+}$ T cell infiltrating and antitumor effects. It is worth noting the sharp outcome distinctions between the oral NP and *i.v.* NP, which could be explained by the different pharmacokinetic profiles of the administration routes, as evidenced by the lower plasma concentrations in Fig. S57. Overall, these data indicated the potential application of synergistic NP to augment immunotherapy, providing a possible therapeutic strategy for turning cold tumors hot. Oral NP"C12 + lomi" was prone to disassociate in the digestive system due to degradation by stomach acids and proteases, ultimately becoming free small molecules.

Discussion

The restoration of chemokine CCL4 presents a promising avenue for ICI therapy, aiming to transform cold tumors into hot ones. Several strategies to upregulate CCL4 have been tested, but none have been successfully been translated into marketed drug forms for clinical use. The limited clinical application of chemokines is primarily due to cytokine/chemokine-induced irAEs [7–9]. These limitations may arise from the on-target toxicity of chemokines, which occurs when the drug engages its intended protein target in healthy tissue, leading to toxic side effects. For instance, the collagen-binding domain-based direct delivery of CCL4 (CBD-CCL4) by Williford et al. presents the risk of potentially accumulating at non-tumor sites with exposed collagen, such as wounds, potentially triggering off-target adverse events like cytokine storms [50].In contrast to the drawbacks of biologics, which include immunogenic sensitivity, prolonged

circulating half-life, limited tissue and tumor penetration, and lack of oral bioavailability, the two small molecules used in the present study, NCTD-C12 and lomi, stand out due to their lower immunogenicity and excellent safety and biocompatibility in tumor-bearing mice.

In contemporary clinical practice, synergy among various small molecules has the potential to enhance the therapeutic index of drugs. However, a significant challenge lies in achieving the co-delivery and synergy of small molecules to maximize the potential of immunotherapy. Although traditional nanomedicine delivery faces challenges such as low EPR effect and tumor tissue heterogeneity [51]. Advanced biomaterials and drug delivery systems play a crucial role in delivering drugs efficiently, improving their efficacy while minimizing toxic side effects. In this study, the NP"C12 + lomi" successfully co-encapsulation of lipophilic NCTD-C12 and lomi within the hydrophobic core of the nanoparticles through the self-assembly of lipid materials, thereby enabling both co-delivery and synergistic effects of small molecules. Meanwhile, due to the tumor-homing ability of the surface-modified RGD peptide, facilitated the specific accumulation of NP"C12 + lomi" in the tumor tissues, significantly reducing toxicity and side effects on normal tissues by ensuring targeted interaction with the intended protein.

NCTD-C12 and lomi are both inhibitors of PP2A. and by inhibiting PP2A, they enhance the stability of the β-catenin degradation of β-catenin [21]. The Wnt/β-catenin signaling pathway plays a crucial role in the self-renewal of CSCs, making it an important therapeutic target in cancer treatment. Compared to other CSC-related signaling pathways, targeting the Wnt/β-catenin pathway has shown more promising therapeutic effects [52]. However, β-catenin has long been considered an "undruggable" target, limiting its application in clinical therapy [53]. Traditionally, the co-delivery of cytotoxic drugs (such as paclitaxel) aims to achieve synergistic effects through two distinct targets [54], effectively killing tumor cells. However, this strategy often enhances cancer stem cell properties and may lead to immune suppression [55]. In contrast, our study addresses this challenge using a non-cytotoxic approach by regulating β-catenin through a small-molecule co-loaded nanoparticle system. By upregulating the expression of chemokines, β-catenin phosphorylation is converted into a non-phosphorylated state, effectively reversing tumor immune escape. This mechanism enhances immune surveillance in tumors, offering a more effective and safer alternative compared to cytotoxic drug-based strategies. The co-localization of synergistic drug pairs at specific sites is crucial for their ability to modulate CCL4. The nanoparticle co-delivery strategy presented in this study offers at least two advantages for this small molecule pair in modulating CCL4.

(1) Physiochemical Stability. A significant challenge in combination drug therapy is determining the optimal manner in which multiple components should be administered to achieve the best outcomes [25]. Small molecule drugs vary widely, ranging from lipophilic to water-soluble compounds. To co-encapsulate substances with divergent lipophilicity within a common nanosystem, two established strategies are often employed. The first strategy involves nanocarriers comprising both lipophilic and hydrophilic elements to facilitate effective interactions with various compounds [56–58]. The second strategy involves modifying drugs into prodrugs, thereby enhancing their compatibility with the delivery system, as exemplified by the conversion of oxaliplatin into a prodrug with an axial carboxyl group for improved encapsulation [59]. In our study, we synthesized NCTD-C12 to bridge the lipophilicity gap when combined with lomi, given their similar LogP values predicted by Discovery Studio™ software (Fig. 3B), which allows them to have similar release behaviors from the nanoparticles. As a prodrug, a portion of NCTD-C12 could be enzymatically converted into NCTD in both in vitro and in vivo. Importantly, molecular docking experiments for NCTD-C12 revealed similar interaction energies between the NCTD parent molecule and the NCTD-C12 prodrug, suggesting that structural modifications did not compromise the pharmacological properties of NCTD.

(2) Pharmacological advantage. The pharmacological advantage of co-encapsulating drugs within NPs is pivotal for delivering multiple agents targeting diverse sub-cellular levels effectively [57]. For example, Triolimus, a micelle co-loaded with paclitaxel, rapamycin, and 17-AAG, exemplifies how co-encapsulation within a single nanocarrier can achieve synergism against multiple cancer cell lines by targeting diverse cellular pathways [60]. Paclitaxel, a mitotic inhibitor, exhibits enhanced cytotoxicity when combined with rapamycin, which inhibits p70s6k phosphorylation, the mechanistic target of rapamycin (mTOR). Additionally, 17-AAG blocks the compensatory Akt pathway activated upon rapamycin treatment. Thus, this triple drug combination requires coordinated delivery within the same NP to achieve synergism by simultaneously blocking both p70s6k and Erk1/2 phosphorylation [60]. Similar studies have shown that Wnt/β-catenin signaling plays a key role in tumor immune escape, which further supports that the drug combinations in our study may improve therapeutic efficacy by affecting this signaling pathway [61]. NCTD suppresses CSC-like properties by inhibiting β-catenin activity [24]. However, standalone NCTD application doesn't sufficiently upregulate CCL4 expression in tumor cells. Remarkably, lomi attenuates CSC-like properties [23], but faces the same problem of poor efficacy when used alone, making it a valuable complementary

agent alongside NCTD in our investigation. As compared to physically mixed free drugs, co-encapsulated NP"C12 + lomi" significantly up-regulated CCL4 expression and attenuated CSC-like properties, owing to the co-encapsulation in nanoparticles allowing them to co-localize and work synergistically.

Selecting the right small-molecule combination is crucial for NP-mediated chemokine regulation. Based on the involvement of Wnt/β-catenin signaling in cytokine regulation [62], this approach may extend to various chemokine and cytokine classes. As research increasingly explores cytokine-ICI combinations [63], our study enhances understanding of a new paradigm in chemokine treatment. It also offers key insights for designing nanomedicine with synergistic small-molecule combinations for ICI therapy, advancing this field.

Conclusions

In summary, our research has resulted in the design of a chemokine-eliciting NP with significant potential for immunotherapy. Within the TME, chemokines are pivotal in regulating immune cell trafficking and shaping the immune landscape. However, systemic administration of chemokines is hindered by the risk of widespread toxicities, necessitating precise control over their expression specifically within the tumor site. This challenge has impeded the clinical translation of chemokine-based therapies, leaving the generation of chemokines through small-molecule drugs relatively unexplored. Our study hypothesized that the NP functions as a modulator, enhancing CCL4 expression through the synergistic action of the "NCTD prodrug + lomi" combination, which deactivates β-catenin. This synergistic mechanism is disrupted upon NP disassociation, leading to the cessation of CCL4 expression. This proof-of-concept study introduces an innovative NP-triggered approach for site-specific CCL4 elicitation, mitigating the risk of irAEs caused by random chemokine distribution. Co-formulating the NCTD prodrug with lomi within the NP emerges as a highly promising strategy for advancing small-molecule therapies. Our research not only expands the horizons of chemokine-based immunotherapy but also provides a foundation for further investigations into precisely controlled chemokine expression, thereby enhancing the efficacy and safety of cancer immunotherapies.

Materials and methods

Materials

Compound Norcantharidin (NCTD) was purchased from Weikeqi-biotech Inc. Ltd., China. Compound PEG_{2000}-DSPE, lomi, *n*-Butyl alcohol, *n*-Hexyl alcohol, *n*-Octanol, *n*-Decyl alcohol, and 1-Dodecanol were purchased from Shanghai Aladdin Bio-Chem Technology Co., Ltd., China. Lecithin was purchased from Alfa Aesar, China. Roswell Park Memorial Institute (RPMI) 1640 medium, Dulbecco's modified eagle medium (DMEM), FBS, L-Glutamine, penicillin/streptomycin cocktail, B27, 0.05% and 0.25% Trypsin were purchased from Gibico, China. TESCA buffer, 10 mM NaAc buffer, normal melting point agar, lower melting point agar, dispase II and collagenases IV were purchased from Solarbio, China. DNase/RNase Deionized Water were purchased from TIANGEN, China. Isopropanol was purchased from Sangon Biotech Co. (Shanghai, China). Universal SYBR Green qPCR Supermix were purchased from US EVERBRIGHT INC, China. Cathepsin B (Cat. No. C6286) was purchased from Sigma-Aldrich, USA. Anti-mouse CD45-FITC antibody, Anti-mouse CD3-APC/eFluor780 antibody, Anti-mouse CD4-APC antibody, Anti-mouse CD8-PerCP antibody, Anti-mouse CD25-eFluor450 antibody, Anti-mouse CD11b-APC/eFluor780 antibody, Anti-mouse CD11c-APC antibody, Anti-mouse GR1-PerCP antibody, Anti-mouse F4/80-eFluor450 antibody, Triton-X-100 were purchased from Thermo Scientific and BioLegend, USA. Compound BMS1016 was customized from Beijing Fuda Inc. Ltd., China. BSA, DAPI, DiO and DiI were purchased from Biyuntian Biotechnology, China.

Animals

SD rats, balb/c mice were acquired from Speiford Beijing Biotechnology Co., Ltd (Beijing, China). All animal study protocols were reviewed and approved by the Animal Ethical Committee at Tianjin University of Traditional Chinese Medicine and adhered to the animal care guidelines of the Laboratory Animal Management Committee.

Cell line and culture

4T1 cell line, E0771 cell line and A549 cell line was purchased from National Collection of Authenticated Cells Culture, China. 4T1 cells were grown in RPMI 1640 medium supplemented with 5% FBS, 1% penicillin/streptomycin, 1 mM Sodium Pyruvate and 0.4 mM Glutamine and maintained at 37 , 5% CO_2. E0771 cells were grown in DMEM medium supplemented with 10% FBS, 1% penicillin/streptomycin, 1 mM Sodium Pyruvate and 0.4 mM Glutamine and maintained at 37 , 5% CO_2.

Western blot analysis

Cells were lysed using lysis buffer following our published protocol [64]. The cell lysates were then applied to the bicinchoninic acid assay (Bio-Rad) to determine protein concentrations, followed by SDS polyacrylamide gel electrophoresis (20–30 mg of protein/lane). The separated proteins were then transferred to polyvinylidene fluoride membrane (PVDF, Millipore, Massachusetts). 5% non-fat dry milk in PBS was applied for the blocking step before primary antibody incubation. The following primary

antibodies were used: anti-total-β-catenin, anti-active-β-catenin (Cell Signaling Technology, US) (dilution 1:1000), and anti-E-cadherin (Cell Signaling Technology, US) (dilution 1:1000), anti-b-actin (Proteintech, US) (dilution 1:8000), the antibody dilution was prepared in PBS containing 1% BSA. After overnight primary antibody incubation at 4 °C, the membranes were washed (The washing buffer consisted of PBS with 0.1% Tween 20, pH 7.4, and was used to wash the samples three times, each for 5 min) and then incubated with HRP-conjugated antibodies (Biosharp, China) for 1 h at room temperature. Images were developed by BioRad ChemiDoc^{MP} Imaging System.

qPCR analysis

Total RNAs were extracted using the Trizol reagent (Invitrogen) and RNA concentrations were measured using NanoDrop™ One (Thermo Scientific). The cDNA was synthesized using the SuperScript™ II RT (Invitrogen) for qPCR amplification, which was carried out in ABI QuantStudio 3 System using ABI TaqMan gene expression assay. The GAPDH level was analyzed and used to normalize specific gene mRNA expression levels as described in our previous study [64]. The primers used in this study were previously reported [46], where their efficiency and specificity were validated. Briefly, qPCR was performed using these primers, with amplification conditions as follows: an initial denaturation and Taq activation at 94 °C for 10 min, followed by 35 cycles of denaturation at 94 °C for 1 min and annealing/extension at 56 °C, concluding with a final elongation at 72 °C for 10 min. The primer sequences in the PCR were shown as follows:

Gene	Primer sequence	Base number
M-GAPDH-F	GGTG AAGG TCGG TGTG AACG	20
M-GAPDH-R	CTCG CTCC TGGA AGAT GGTG	20
M-CCL4-F	TTCC TGCT GTTT CTCT TACA CCT	23
M-CCL4-R	CTGT CTGC CTCT TTTG GTCA G	21

Soft agar colony formation assay

The soft agar colony formation experiment was performed in 60-mm tissue culture dishes following our previous protocol [24]. Cells were collected by trypsinization and suspended in culture media at a concentration of 0.5×10^3 cells mL^{-1}. Four milliliters of 0.6% normal melting point agar, were placed into each 60-mm tissue culture dish as the bottom agar. The preparation of the agar solution followed standard procedures: a suitable amount of agar was weighed and dissolved in water, then sterilized in an autoclave. Two milliliter of cell suspension (0.5×10^3 cells mL^{-1}) and 2 mL of 0.8% lower melting point agar, and each treatment (NCTD, lomi and NCTD + lomi) were mixed and poured over the bottom agar. The control group underwent the same procedures as the treated group, except for the omission of the drug, and each group was repeated in triplicate. After solidification of this upper agar, 3 mL of culture media were added, and dishes were incubated at 37 °C in a humidified 5% CO_2 atmosphere. Colony formation in the agar was fixed by methanol and then stained with 0.33% (w/v) crystal violet solution, imaged, and counted after 4-week culture.

The synthesis and characterization of NCTD prodrugs-C4, C6, C8, C10, C1

To a solution of Norcantharidin (1.0 g, 5.95 mmol) in *n*-Butyl alcohol (4 mL) was added H_2SO_4 (0.1 mL) at r.t. The mixture was refluxed for 65 min at 80 °C. Then the reaction mixture was cooled to r.t., washed with H_2O (3 × 10 mL), and filtered to give a white waxy solid. The solid was recrystallized with *n*-hexane and filtered to give compound C4 (1.0 g, 3.36 mmol, 56%) as a white solid.

^{1}H NMR (400 MHz, $CDCl_3$) δ 4.91–4.84 (m, 2 H), 4.14–3.95 (m, 4 H), 2.95 (s, 2 H), 1.83–1.76 (m, 2 H), 1.60–1.49 (m, 6 H), 1.40–1.30 (m, 4 H), 0.91 (dd, *J* = 9.2, 7.5 Hz, 6 H).

To a solution of Norcantharidin (1.0 g, 5.95 mmol) in *n*-Hexyl alcohol (4 mL) was added H_2SO_4 (0.1 mL) at r.t. The mixture was refluxed for 65 min at 80 °C. Then the reaction mixture was cooled to r.t., washed with H_2O (3 × 10 mL), and filtered to give a white waxy solid. The solid was recrystallized with *n*-hexane and filtered to give compound C6 (1.1 g, 3.11 mmol, 52%) as a white solid.

^{1}H NMR (400 MHz, $CDCl_3$) δ 4.88 (dd, *J* = 3.3, 2.3 Hz, 2 H), 4.10–3.95 (m, 4 H), 2.95 (s, 2 H), 1.84–1.75 (m, 2 H), 1.61–1.49 (m, 6 H), 1.34–1.24 (m, 12 H), 0.87 (t, *J* = 7.8 Hz, 6 H).

To a solution of Norcantharidin (1.0 g, 5.95 mmol) in *n*-Octanol (4 mL) was added H_2SO_4 (0.1 mL) at r.t. The mixture was refluxed for 65 min at 80 °C. Then the reaction mixture was cooled to r.t., washed with H_2O (3 × 10 mL), and filtered to give a white waxy solid. The solid was recrystallized with *n*-hexane and filtered to give compound C8 (1.2 g, 2.92 mmol, 49%) as a white solid.

^{1}H-NMR (DMSO-*d6*, 400 MHz): δ 4.65–4.64 (m, 2 H), 3.92–3.80 (m, 4 H), 3.03 (s, 2 H), 1.53–1.44 (m, 8 H), 1.24–1.21 (m, 20 H), 0.82 (t, *J* = 6.8 Hz, 6 H).

To a solution of Norcantharidin (1.0 g, 5.95 mmol) in *n*-Decylalcohol (4 mL) was added H_2SO_4 (0.1 mL) at r.t. The mixture was refluxed for 60 min at 100 °C. Then the reaction mixture was cooled to r.t., washed with H_2O (3 × 10 mL), and filtered to give a white waxy solid. The solid was recrystallized with *n*-hexane and filtered to give compound C10 (1.7 g, 3.64 mmol, 61%) as a white solid.

^{1}H-NMR (DMSO-*d6*, 400 MHz): δ 4.65–4.64 (m, 2 H), 3.92–3.80 (m, 4 H), 3.03 (s, 2 H), 1.53–1.45 (m, 8 H), 1.23–1.21 (m, 28 H), 0.82 (t, *J* = 6.8 Hz, 6 H).

To a solution of Norcantharidin (0.6 g, 3.57 mmol) in 1-Dodecanol (3 mL) was added H_2SO_4 (0.1 mL) at r.t. The mixture was refluxed for 60 min at 100 °C. Then the reaction mixture was cooled to r.t., washed with H_2O (3 × 10 mL), and filtered to give a white waxy solid. The solid was recrystallized with *n*-hexane and filtered to give compound C12 (1.3 g, 2.49 mmol, 70%) as a white solid.

^{1}H-NMR (DMSO-*d6*, 400 MHz): δ 4.89–4.87 (m, 2 H), 4.09–3.96 (m, 4 H), 2.95 (s, 2 H), 1.81–1.49 (m, 8 H), 1.28–1.24 (m, 36 H), 0.87 (t, *J* = 6.8 Hz, 6 H).

All compounds were dissolved in dimethyl sulfoxide for in vitro treatments or further experiments.

Molecular Docking

The structure of the Protein Phosphatase 2 A Core Enzyme (PDB ID: 2IE4) was selected for molecular docking. The protein structure was processed by the Protein Preparation module in Discovery Studio 2019, wherein all water molecules were removed and all other parameters were set to default. A spherical region with a 11 Å diameter was established as the active site [65], centered on the ligand molecule. To select the best docking poses for further analysis, we considered the docking scores and the binding interactions with key residues of the target protein. Poses with the lowest binding energies (i.e., most negative docking scores) and stable interactions with the active site were selected for further analysis. Additionally, poses were evaluated for consistency across multiple docking runs. The docking simulations were conducted using the CDOCKER module, and the top-10 poses of each compound were saved for further analysis. To validate the docking method, we re-docked a known ligand (okadaic acid, a previously reported inhibitor [66]) into the receptor binding site, and the result was consistent with experimentally observed binding modes.

Preparation and characterization of NP

RGD-PEG_{2000}-DSPE was obtained by the same method as described previously [24]. Briefly, Mal-PEG-DSPE and RGD-SH (molar ratio 1:1.5) were dissolved in 0.05 M HEPES/0.01 M EDTA aqueous solution and rotated overnight at room temperature in the dark. At the end of the reaction, ultrafiltration was performed to remove excess free RGD-SH peptide. Then, lomi, NCTD-C12, lecithin, PEG_{2000}-DSPE, and RGD-PEG_{2000}-DSPE were dissolved in chloroform ($CHCl_3$) solution. Meanwhile, a certain amount of water was added to the above organic phase solution, the vortices were fully formed after the two solutions were mixed. And then they were homogenized by a high-pressure homogenizer (ATS, Canada) for half an hour. After removing the residual chloroform, the nanoparticles were left to self-assemble at room temperature overnight. Finally, the remaining free molecules were removed by an Amicon Ultra-4 centrifugal filter (Molecular cut-off 100,000, Millipore, Billerica, MA, US) and then resuspended in 0.9% saline to obtain a final desired concentration. The diameter and zeta potential of these nanoparticles were characterized by a Zetasizer Nano ZS90 (Malvern, UK). Transmission electron microscopy (TEM) was performed using a Hitachi H-7800 (Hitachi, Japan). The samples were placed on copper grids and negatively stained with 2% phosphotungstic acid (PTA) for enhanced contrast. The samples were observed at an acceleration voltage of 80 kV, and images were captured using a CCD camera. The morphology of the nanoparticles was analyzed by measuring the size distribution and shape from the obtained images.

The content determination of C12 and Lomi by LC-MS/MS

Generally, C12 and lomi content in NP"C12 + lomi" solution and EE% were determined by LC-MS/MS method. A UPLC I-Class system (Waters Corp., Milford, MA, USA) interfaced with a XEVO TQ-MS mass spectrometer (Waters, USA) equipped with electrospray ionization (ESI) source were used in the study. The separation was performed on an Acquity UPLC BEH C18 column (2.1 × 50 mm, 1.7 μm). The flow rate was 0.4 mL min^{-1}, and the mobile phase consisted of 0.1% formic acid in water (solvent A) and 0.1% formic acid in acetonitrile (solvent B). The gradient elution conditions were as follows: 0–1 min, 90% A; 1–3 min, 90%–0% A; 3–5 min, 0% A; 5–6 min, 0 – 90% A; 6–8 min, 90% A. And the injection volume was 4 μL. lomi and C12 were monitored in positive mode with multiple reactions monitoring. The precursor-to-product ion transition of lomi and C12 were *m/z* 694→249 and 523→169, respectively. Briefly, nanoparticle solutions were diluted at 1:1 ratio with acetone and then 1 M NaOH solution was added at 1:1 ratio after complete evaporation of acetone. The solutions were finally vortexed to release free drug from the ionic complexes. After centrifugation (10000 rpm × 5 min), supernatant was diluted by mobile phase and injected to the LC-MS/MS for quantification. C12 and lomi peak from nanoparticle solutions were quantified by comparing to a calibration curve of known C12 and lomi concentration standard and corrected to account for sample dilution. The weight ratio of entrapped drug to added drug was defined as the encapsulation efficiency (EE%). The encapsulation efficiency (EE%) was calculated using the following formula: EE% = (1- Free Drug/Total Drug) × 100%.

Measurement of C12 and NP"C12 + lomi" responsive toward cathepsin B

C12 and NP"C12 + lomi", was dispersed separately in solution in 1 mL sodium acetate buffer solution (pH 5.0) contained cathepsin B (U-activity unit = 10 U mL^{-1}) for 72 h. The samples were kept in isothermal shaker at 37

and 100 rpm. At the predetermined time point, 100 μL of the sample solution was withdrawn, and same amount of acetonitrile was added immediately. The accumulative drug release was measured by LC-MS/MS.

The amount of NCTD and NCTD-C12 presenting in tumor tissue

Orthotopic mammary homograft tumors were established by injecting 5×10^5 4T1 cells directly into the 4th mammary gland fat pad, using a similar method described previously. NCTD-C12 was administered via intratumoral injection (i.t.) at a dosage of 10 mg kg^{-1} following tumor growth to ≈100 mm^3 for 72 h. After surgery, collected tumor tissue, added three times the volume of water for homogenization, then pipetted an appropriate amount of homogenate, added acetone, fully vortex and mix, centrifuge at 12,000 rpm at 4 °C for 10 min, took the supernatant, nitrogen was used as the drying gas, add methanol, vortex and shake. The amounts of NCTD and NCTD-C12 was determined by LC-MS/MS method.

Determination of drug release profile

Drug release profiles of NP"C12 + lomi" were determined using a dialysis method. To test C12 or lomi release, lyophilized NP"C12 + lomi" (2.5 mg) was dispersed in 0.4 ml of PBS and transferred to the dialysis bag (MWCO: 10 K). The dialysis bag was immersed into a 250 mL glassware containing 200 mL PBS (1% Tween 20) and incubated in a water bath at 37 °C under stirring condition. The amounts of drug released at the determined time points was determined by LC-MS/MS.

Determination of NP stability

DiO-DiL-labeled nanoparticles (DiO-DiL-NP"C12 + Lomi") and FITC-Dil-NP"C12 + Lomi" were prepared according to the procedure described in the preceding steps for preparing nanoparticles. The nanoparticles were then dialyzed in PBS (pH 7.4) at 37 °C with continuous shaking at 100 rpm to simulate in vivo drug release conditions. Samples were taken at various time points (0, 15, 30 min, 1, 2, 4 and 8 h) to measure the fluorescence intensity and calculate the FRET efficiency, which indicates the release and energy transfer dynamics between the donor and acceptor molecules within the nanoparticles. According to the fluorescence intensity of the spectrum, the change of FRET efficiency of micelles at each time was calculated according to the following formula: EffFRET (%) = IR/(IG + IR) [EffFRET: FRET efficiency; IR: Fluorescence intensity of DiI at 565 nm; IG: Fluorescence intensity of DiO at 501 nm (in DiO-DiL-NP"C12 + Lomi") or fluorescence intensity of FITC at 525 nm (in FITC-Dil-NP"C12 + Lomi)]

In vitro cytotoxicity assay

An MTT assay was performed to evaluate the in vitro cytotoxicity. Briefly, cells were seeded on 96-well plates ($3 \sim 5 \times 10^3$ cells/well in 100 μL of complete culture medium). Different concentrations of polymers or NPs were added into the wells 24 h after cell seeding and incubated with cells for 48 h; saline or dimethyl sulfoxide (DMSO) was used as a positive control. At the end of incubation, 50 μL of the MTT reagent (5 mg mL^{-1}) was added to each well and incubated for 4 h. Then, 200 μL of DMSO was added to each well and incubated for another 1 h. The plate was recorded using a microplate reader (SpectraMax i3x, Molecular Devices, Sunnyvale, CA, USA) at the wavelength of 570 nm. The inhibition of relative cell growth was determined by the following formula: Cell Viability (%) = (Absorbance at 570 nm of NP treated cells) / (Absorbance at 570 nm of control – treated cells) × 100%.

Hemolysis assay

Preparation of Physiological Saline: 0.9 g of sodium chloride (NaCl) was dissolved in 99.1 mL of distilled water under continuous stirring to obtain a 0.9% (w/v) physiological saline solution. Preparation of Red Blood Cell Suspension: Fresh mouse blood (6 mL) was collected in a 15 mL centrifuge tube and mixed with an equal volume of physiological saline. The mixture was centrifuged at 3,000 ×g for 5 min at 4 °C. The supernatant was carefully removed, and the RBC pellet was resuspended in an equal volume of physiological saline. This washing process was repeated three times or until the supernatant became colorless. The purified RBCs were diluted with physiological saline in a 50 mL volumetric flask to prepare a 2% (v/v) RBC suspension, which was stored at 4 °C for subsequent experiments. Preparation of Sample Solutions: NP blank solution and drug-loaded NP solution (concentration range: 0.125–2 mg/mL) were mixed with an equal volume of the 2% RBC suspension. The mixtures were incubated in a water bath at 37 °C for 2 h, followed by centrifugation at 3,000 ×g for 10 min. The absorbance of the supernatant was measured at 540 nm using a spectrophotometer. Physiological saline and ultrapure water were used as negative (0% hemolysis) and positive controls (100% hemolysis), respectively.

Cell migration assay protocol

4T1 cells in the logarithmic growth phase were seeded into culture dishes and incubated at 37 °C in a 5% CO_2 humidified atmosphere. When cellular confluence reached > 90%, parallel equidistant reference lines were drawn along the dish diameter using a sterile marker pen for orientation. Uniform scratch wounds were subsequently created perpendicular to these reference lines using a 200 μL pipette tip. Following scratch formation, detached cells were

removed by three PBS washes. Cells were then maintained in complete medium containing 10 μg/mL mitomycin C (to inhibit proliferation) and experimental drug treatments at specified concentrations. Phase-contrast images of wound closure progression were captured at 0, 6, 24, and 48 h time points using an inverted microscope equipped with digital imaging system.

Immunofluorescence staining

Paraffin sections of tumor tissues were dewaxed in sequential series of solutions: 100%, 95%, 80%, 70%, and 50% ethanol (each for 2 min), followed by a rinse in a distilled water for 10 min and then in 1 × PBS for 10 min. The slide rack was then placed in a beaker containing the retrieval solution and autoclaved at 121 with 15 Psi for 20 min. After natural cooling, slides were rinsed twice in PBS for 5 min. Subsequently, closure solution (2% BSA, 0.1% Triton-X-100 in PBS solution) was prepared and incubated for 30 min. Primary antibody solution was prepared by diluting β-catenin to a 1:200 concentration with the blocking solution and then incubated overnight at 4 in a light protected, humidified container. Secondary antibody solution was prepared at a 1:300 ratio with 1 × PBS and incubated for 1 h at room temperature, followed by two rinses with PBS (5 min). Finally, DAPI solution was added and incubated for 10 min at room temperature, rinsed once with PBS for 5 min, and the slides were then mounted with a cover slip.

Suspension culture spheroid formation assay

The spheroid formation assay was performed following the published protocol with minor modifications [64]. Briefly, single 4T1 cells were plated in ultralow attachment 48-well culture plates at a density of 2×10^3 cells per well suspended in serum-free RPMI 1640 medium containing human recombinant basic fibroblast growth factor (20 ng mL^{-1}), human recombinant epidermal growth factor (20 ng mL^{-1}), 1% penicillin/streptomycin, B27 supplement (1/50, v/v) and heparin (4 mg mL^{-1}). Plates were incubated at 37 °C in cell incubator with 5% CO_2. Spheres > 50 mm were viewed and photographed under a phase-contrast microscope after 10-day culture.

Evaluation of the therapeutic effect of systemic administration of NP on TNBC using a mouse orthotopic mammary homograft tumor model

The orthotopic mammary homograft tumors were established by directly injecting 0.5 million of 4T1 cells into the 4th mammary gland fat pad as the similar method described previously [24]. The treatment began on day 8 post 4T1 cell inoculation. NP"C12 + lomi" was administered *i.v.* or orally at the dosages of C12 (20 mg kg^{-1}) body weight and lomi (10 mg kg^{-1}) body weight; BMS1016 was prepared in Cremophor vehicle (Cremophor EL/ethanol 1:1, diluted 1:4 with PBS after the addition of BMS1016) was administered *i.p.* at the dosage of 1 mg kg^{-1} body weight; PBS and NP blank were set as controls. On day 36 post 4T1 cell inoculation, all mice were euthanized. The lungs were harvested and collected. After immersion with Bouin's fixative for 24 h, the metastatic nodules on the surface of the lungs were counted and then the lungs were imaged individually. The mammary tumors were collected and weighted.

Flow cytometry

Single-cell dissociation from tumor tissue and the following flow cytometry analysis of immune cells were performed as below. Briefly, the tumor fraction was cut into pieces by manually mincing the tissues using scissors, followed by enzymatic digestion with 4 mg mL^{-1} collagenase IV (Roche, UK), 0.375 mg mL^{-1} dispase II, and 0.6% FBS for 60 min at 37 °C with gentle stirring. The digested samples were filtered through 70 mm cell strainer and centrifuged at 1600 rpm for 3 min. The cells were then incubated in labeling medium containing antibodies for 30 min in the dark. After that, cells were washed and resuspended in PBS containing 0.1% FBS and proceeded to flow cytometry analysis, and all flow plots represent live, single cells, with 100,000 events.

In vivo bioluminescence imaging

Bioluminescence imaging (BLI) was performed at the indicated time points using an IVIS Lumina III in vivo imaging system (PerkinElmer). Analysis was performed using Living Image 4.3.1 software (Caliper Life Sciences). Mice underwent intraperitoneal injection with luciferin (150 mg kg^{-1}; Promega) and were imaged (exposed time: Auto) under isoflurane anesthesia after 10 min. Animals were inspected daily and killed when experimental endpoints had been achieved or when symptomatic due to tumor progression. The mice were anesthetized by isoflurane and further performed the surgical dissection.

Assessment of Lomi and NCTD-C12 pharmacokinetics

Twelve female SD rats were randomly divided into two groups, one group received a single intragastric gavage (i.g.) administration of lomi and C12 in NP, and the other group was by intravenous injection (*i.v.*). Each rat was given a single dose of C12 20 mg kg^{-1} body weight and lomi 10 mg kg^{-1} body weight, fasted for 12 h before administration, drank freely, and crossed after a cleaning period of 1 week. Blood samples were collected into heparinized Eppendorf tubes from fossa orbitalis vein at 0.083, 0.167, 0.333, 0.5, 1, 2, 4, 8, 12, 24, 48, 72 and 96 h after administration, and then immediately centrifuged at 3500 rpm min^{-1} for 10 min. The supernatants were separated and stored at -80 °C until analysis. The concentrations of C12 and lomi in blood plasma were quantified using HPLC-MS.

Statistical analysis

For in vitro and rodent studies, all quantitative measurements were performed on at least three independent replicates. All values are expressed as means ± SD. Statistical analysis was performed using GraphPad Prism 8. $^{*}P < 0.05$, $^{**}P < 0.01$, $^{***}P < 0.001$ was considered statistically different. Survival benefit was determined using a log-rank test. Biological replicates were used in all experiments unless otherwise stated.

Supplementary Information

The online version contains supplementary material available at https://doi.org/10.1186/s12951-025-03425-8.

Supplementary Material 1

Acknowledgements

This research was funded by Tianjin University of Traditional Chinese Medicine Startup Funding to Yunfei Li, and supported by Open Projects Fund of Shandong Key Laboratory of Carbohydrate Chemistry and Glycobiology, Shandong University (No. 2023CCG13), and the Jilin Province Science and Technology Development Plan Item (YDZJ202501ZYTS818), and CAMS Innovation Fund for Medical Sciences (CIFMS) (2021-I2M-1-026, China).

Author contributions

F.Z., L.G. and P.W. designed and performed the experiments, analyzed the data, and wrote the original draft. D.C., S.C., Y.L. and F.Y. contributed to the animal experiments and edited the manuscript. M.T., Y.M. and Y.W. assisted with the data analysis. L.M., Y.L. and W.H. supervised the research, conceived the overall concept and reviewed and edited the manuscript. All authors discussed the test results and provided comments on the manuscript.

Data availability

No datasets were generated or analysed during the current study.

Declarations

Ethics approval and consent to participate

The experimental protocol concerning animals used in this work was approved by the Animal Ethical Committee at Tianjin University of Traditional Chinese Medicine and adhered to the animal care guidelines of Laboratory Animal Management Committee (Approval TCM-LAEC2023114).

Consent for publication

All authors involved in this study have provided their consent for the publication of the research findings.

Competing interests

The authors declare no competing interests.

Author details

[1]College of Chinese Materia Medica, Tianjin University of Traditional Chinese Medicine, Tianjin 301617, China
[2]State Key Laboratory of Bioactive Substance and Function of Natural Medicines, Institute of Materia Medica, Chinese Academy of Medical Sciences and Peking Union Medical College, Beijing 100050, China
[3]Suzhou Kintor Pharmaceuticals, Inc., Suzhou 215127, China
[4]State Key Laboratory of Component-Based Chinese Medicine, Tianjin University of Traditional Chinese Medicine, Tianjin 301617, China
[5]Key Laboratory of Bioactive Substances and Resources Utilization of Chinese Herbal Medicines, Ministry of Education, Institute of Medicinal Plant Development, Chinese Academy of Medical Sciences & Peking Union Medical College, Beijing 100193, PR China
[6]Shandong Key Laboratory of Carbohydrate Chemistry and Glycobiology, Shandong University, Jinan, China

Received: 13 November 2024 / Accepted: 1 May 2025
Published online: 21 May 2025

References

1. Spranger S, Bao R, Gajewski TF. Melanoma-intrinsic β-catenin signalling prevents anti-tumour immunity. Nature. 2015;523:231–5.
2. Spranger S, Dai D, Horton B, Gajewski TF. Tumor-Residing Batf3 dendritic cells are required for effector T cell trafficking and adoptive T cell therapy. Cancer Cell. 2017;31:711–e723714.
3. Ozga AJ, Chow MT, Luster AD. Chemokines and the immune response to cancer. Immunity. 2021;54:859–74.
4. Cheng NL, Chen X, Kim J, Shi AH, Nguyen C, Wersto R, Weng NP. MicroRNA-125b modulates inflammatory chemokine CCL4 expression in immune cells and its reduction causes CCL4 increase with age. Aging Cell. 2015;14:200–8.
5. Honey K. CCL3 and CCL4 actively recruit CD8 + T cells. Nat Rev Immunol. 2006;6:427–427.
6. Bystry RS, Aluvihare V, Welch KA, Kallikourdis M, Betz AG. B cells and professional apcs recruit regulatory T cells via CCL4. Nat Immunol. 2001;2:1126–32.
7. Liu J-Q, Zhu J, Hu A, Zhang A, Yang C, Yu J, Ghoshal K, Basu S, Bai X-F. Is AAV-delivered IL-27 a potential immunotherapeutic for cancer? Am J Cancer Res. 2020;10:3565.
8. Car BD, Eng VM, Schnyder B, LeHir M, Shakhov AN, Woerly G, Huang S, Aguet M, Anderson TD, Ryffel B. Role of interferon-gamma in Interleukin 12-induced pathology in mice. Am J Pathol. 1995;147:1693.
9. Ryffel B. Interleukin-12: role of interferon-γ in IL-12 adverse effects. Clin Immunol Immunopathol. 1997;83:18–20.
10. Lasek W, Zagożdżon R, Jakobisiak M. Interleukin 12: still a promising candidate for tumor immunotherapy? Cancer Immunol Immunother. 2014;63:419–35.
11. Yang J, Hu L. Immunomodulators targeting the PD-1/PD-L1 protein-protein interaction: from antibodies to small molecules. Med Res Rev. 2019;39:265–301.
12. Bailly C, Vergoten G. Protein homodimer sequestration with small molecules: focus on PD-L1. Biochem Pharmacol. 2020;174:113821.
13. Vladimer GI, Snijder B, Krall N, Bigenzahn JW, Huber KV, Lardeau C-H, Sanjiv K, Ringler A, Berglund UW, Sabler M. Global survey of the Immunomodulatory potential of common drugs. Nat Chem Biol. 2017;13:681–90.
14. Adams JL, Smothers J, Srinivasan R, Hoos A. Big opportunities for small molecules in immuno-oncology. Nat Rev Drug Discovery. 2015;14:603–22.
15. Spranger S, Dai D, Horton B, Gajewski TF. Tumor-residing Batf3 dendritic cells are required for effector T cell trafficking and adoptive T cell therapy. Cancer Cell. 2017;31:711–23. e714.
16. Ganesh S, Shui X, Craig KP, Park J, Wang W, Brown BD, Abrams MT. RNAi-mediated β-catenin Inhibition promotes T cell infiltration and antitumor activity in combination with immune checkpoint Blockade. Mol Ther. 2018;26:2567–79.
17. Gajewski T, Spranger S. Beta-catenin inhibitors in cancer immunotherapy. USA: The University of Chicago; 2016. p. 116.
18. Hsu W, Zeng L, Costantini F. Identification of a domain of Axin that binds to the serine/threonine protein phosphatase 2A and a self-binding domain. J Biol Chem. 1999;274:3439–45.
19. Seeling JM, Miller JR, Gil R, Moon RT, White R, Virshup DM. Regulation of β-catenin signaling by the B56 subunit of protein phosphatase 2A. Science. 1999;283:2089–91.
20. Luo W, Peterson A, Garcia BA, Coombs G, Kofahl B, Heinrich R, Shabanowitz J, Hunt DF, Yost HJ, Virshup DM. Protein phosphatase 1 regulates assembly and function of the β-catenin degradation complex. EMBO J. 2007;26:1511–21.
21. Stamos JL, Weis WI. The β-catenin destruction complex. Cold Spring Harb Perspect Biol. 2013;5:a007898.
22. Zuo Q, Liao L, Yao Z-T, Liu Y-P, Wang D-K, Li S-J, Yin X-F, He Q-Y, Xu W-W. Targeting PP2A with lomitapide suppresses colorectal tumorigenesis through the activation of AMPK/Beclin1-mediated autophagy. Cancer Lett. 2021;521:281–93.
23. Yang C, Wang Z, Li Y. Anti-cancer compositions and methods comprising Miriplatin assembled into ultrasmall Dot and/or lomitapide. Volume 107. USA: University of Kentucky Research Foundation; 2021. p. 107pp.
24. Li Y, Xiao Y, Lin H-P, Reichel D, Bae Y, Lee EY, Jiang Y, Huang X, Yang C, Wang Z. In vivo β-catenin Attenuation by the integrin α5-targeting nano-delivery strategy suppresses triple negative breast cancer stemness and metastasis. Biomaterials. 2019;188:160–72.

25. Zhang RX, Wong HL, Xue HY, Eoh JY, Wu XY. Nanomedicine of synergistic drug combinations for cancer therapy–Strategies and perspectives. J Controlled Release. 2016;240:489–503.
26. Al Bostami RD, Abuwatfa WH, Husseini GA. Recent advances in Nanoparticle-Based Co-Delivery systems for Cancer therapy. Nanomaterials. 2022;12:2672.
27. Wang Q, Wang Y, Ding J, Wang C, Zhou X, Gao W, Huang H, Shao F, Liu Z. A bioorthogonal system reveals antitumour immune function of pyroptosis. Nature. 2020;579:421–6.
28. Hwang S-Y, Deng X, Byun S, Lee C, Lee S-J, Suh H, Zhang J, Kang Q, Zhang T, Westover KD. Direct targeting of β-catenin by a small molecule stimulates proteasomal degradation and suppresses oncogenic Wnt/β-catenin signaling. Cell Rep. 2016;16:28–36.
29. Al-Hajj M, Wicha MS, Benito-Hernandez A, Morrison SJ, Clarke MF. Prospective identification of tumorigenic breast cancer cells. Proc Natl Acad Sci U S A. 2003;100:3983–8.
30. Rubinfeld B, Robbins P, El-Gamil M, Albert I, Porfiri E, Polakis P. Stabilization of beta-catenin by genetic defects in melanoma cell lines. Science. 1997;275:1790–2.
31. Väyrynen JP, Kantola T, Väyrynen SA, Klintrup K, Bloigu R, Karhu T, Mäkelä J, Herzig KH, Karttunen TJ, Tuomisto A. The relationships between serum cytokine levels and tumor infiltrating immune cells and their clinical significance in colorectal cancer. Int J Cancer. 2016;139:112–21.
32. Ruiz de Galarreta M, Bresnahan E, Molina-Sánchez P, Lindblad KE, Maier B, Sia D, Puigvehi M, Miguela V, Casanova-Acebes M, Dhainaut M, et al. β-Catenin activation promotes immune escape and resistance to Anti-PD-1 therapy in hepatocellular carcinoma. Cancer Discov. 2019;9:1124–41.
33. Shi J, Kantoff PW, Wooster R, Farokhzad OC. Cancer nanomedicine: progress, challenges and opportunities. Nat Rev Cancer. 2017;17:20–37.
34. Carvalho BG, Vit FF, Carvalho HF, Han SW, Lucimara G. Recent advances in co-delivery nanosystems for synergistic action in cancer treatment. J Mater Chem B. 2021;9:1208–37.
35. Liu M, Ma X, Jin Z, Li W, Guo M, Li F. Determination and Pharmacokinetic study of the Diacid metabolite of Norcantharidin in beagle plasma by use of liquid chromatography–tandem mass spectrometry. Anal Bioanal Chem. 2013;405:9273–83.
36. [https://pubchem.ncbi.nlm.nih.gov/compound/Lomitapide#section=Experimental-Properties]
37. Baba Y, Hirukawa N, Sodeoka M. Optically active Cantharidin analogues possessing selective inhibitory activity on Ser/Thr protein phosphatase 2B (calcineurin): implications for the binding mode. Bioorg Med Chem. 2005;13:5164–70.
38. Rautio J, Kumpulainen H, Heimbach T, Oliyai R, Oh D, Järvinen T, Savolainen J. Prodrugs: design and clinical applications. Nat Rev Drug Discovery. 2008;7:255–70.
39. Olson OC, Joyce JA. Cysteine cathepsin proteases: regulators of cancer progression and therapeutic response. Nat Rev Cancer. 2015;15:712–29.
40. Quijano-Rubio A, Bhuiyan AM, Yang H, Leung I, Bello E, Ali LR, Zhangxu K, Perkins J, Chun J-H, Wang W et al. A split, conditionally active mimetic of IL-2 reduces the toxicity of systemic cytokine therapy. Nat Biotechnol 2022;41:532-540.
41. Takeuchi Y, Tanegashima T, Sato E, Irie T, Sai A, Itahashi K, Kumagai S, Tada Y, Togashi Y, Koyama S, et al. Highly Immunogenic cancer cells require activation of the WNT pathway for immunological escape. Sci Immunol. 2021;6:eabc6424.
42. Mitchell MJ, Billingsley MM, Haley RM, Wechsler ME, Peppas NA, Langer R. Engineering precision nanoparticles for drug delivery. Nat Rev Drug Discovery. 2021;20:101–24.
43. Kemp JA, Shim MS, Heo CY, Kwon YJ. Combo nanomedicine: co-delivery of multi-modal therapeutics for efficient, targeted, and safe cancer therapy. Adv Drug Deliv Rev. 2016;98:3–18.
44. Hu J, Sánchez-Rivera FJ, Wang Z, Johnson GN, Ho Y-j, Ganesh K, Umeda S, Gan S, Mujal AM, Delconte RB. STING inhibits the reactivation of dormant metastasis in lung adenocarcinoma. Nature. 2023;616:806–13.
45. Yeung K-S, Grant-Young KA, Zhu J, Saulnier MG, Frennesson DB, Langley DR, Hewawasam P, Wang T, Zhang Z, Meng Z, et al. Preparation of biphenyl compounds useful as immunomodulators for treatment of cancer, infectious diseases, and septic shock. USA: Bristol-Myers Squibb Company; 2018. p. 370.
46. Feng X, Ge J, Fu H, Miao L, Zhao F, Wang J, Sun Y, Li Y, Li Y. Discovery of small molecule β-catenin suppressors that enhance immunotherapy. Bioorg Chem. 2023;139:106754.
47. Du L, Lee J-H, Jiang H, Wang C, Wang S, Zheng Z, Shao F, Xu D, Xia Y, Li J. β-Catenin induces transcriptional expression of PD-L1 to promote glioblastoma immune evasion. J Exp Med 2020;217:e20191115.
48. Lyden D, Ghajar CM, Correia AL, Aguirre-Ghiso JA, Cai S, Rescigno M, Zhang P, Hu G, Fendt S-M, Boire A. Metastasis. Cancer Cell. 2022;40:787–91.
49. de Lara PT, Castañón H, Sterpi M, van den Broek M. Antimetastatic defense by CD8 + T cells. Trends cancer. 2022;8:145–57.
50. Williford J-M, Ishihara J, Ishihara A, Mansurov A, Hosseinchi P, Marchell TM, Potin L, Swartz MA, Hubbell JA. Recruitment of CD103 + dendritic cells via tumor-targeted chemokine delivery enhances efficacy of checkpoint inhibitor immunotherapy. Sci Adv. 2019;5:eaay1357.
51. Azizi M, Jahanban-Esfahlan R, Samadian H, Hamidi M, Seidi K, Dolatshahi-Pirouz A, Yazdi AA, Shavandi A, Laurent S, Be Omide Hagh M, et al. Multifunctional nanostructures: intelligent design to overcome biological barriers. Mater Today Bio. 2023;20:100672.
52. Fendler A, Bauer D, Busch J, Jung K, Wulf-Goldenberg A, Kunz S, Song K, Myszczyszyn A, Elezkurtaj S, Erguen B. Inhibiting WNT and NOTCH in renal cancer stem cells and the implications for human patients. Nat Commun. 2020;11:929.
53. Cui C, Zhou X, Zhang W, Qu Y, Ke X. Is β-catenin a druggable target for cancer therapy? Trends Biochem Sci. 2018;43:623–34.
54. Mukherjee P, Gupta A, Chattopadhyay D, Chatterji U. Modulation of SOX2 expression delineates an end-point for paclitaxel-effectiveness in breast cancer stem cells. Sci Rep. 2017;7:9170.
55. Zou W, Wolchok JD, Chen L. PD-L1 (B7-H1) and PD-1 pathway Blockade for cancer therapy: mechanisms, response biomarkers, and combinations. Sci Transl Med. 2016;8:rv328324–328324.
56. Wong HL, Bendayan R, Rauth AM, Wu XY. Development of solid lipid nanoparticles containing ionically complexed chemotherapeutic drugs and chemosensitizers. J Pharm Sci. 2004;93:1993–2008.
57. Wong HL, Bendayan R, Rauth AM, Wu XY. Simultaneous delivery of doxorubicin and GG918 (Elacridar) by new polymer-lipid hybrid nanoparticles (PLN) for enhanced treatment of multidrug-resistant breast cancer. J Controlled Release. 2006;116:275–84.
58. Shuhendler AJ, Cheung RY, Manias J, Connor A, Rauth AM, Wu XY. A novel doxorubicin-mitomycin C co-encapsulated nanoparticle formulation exhibits anti-cancer synergy in multidrug resistant human breast cancer cells. Breast Cancer Res Treat. 2010;119:255–69.
59. Xiao H, Li W, Qi R, Yan L, Wang R, Liu S, Zheng Y, Xie Z, Huang Y, Jing X. Co-delivery of daunomycin and oxaliplatin by biodegradable polymers for safer and more efficacious combination therapy. J Controlled Release. 2012;163:304–14.
60. Hasenstein JR, Shin H-C, Kasmerchak K, Buehler D, Kwon GS, Kozak KR. Antitumor activity of Triolimus: a novel multidrug-loaded micelle containing Paclitaxel, Rapamycin, and 17-AAG. Mol Cancer Ther. 2012;11:2233–42.
61. Majidinia M, Aghazadeh J, Jahanban-Esfahlani R, Yousefi B. The roles of Wnt/β-catenin pathway in tissue development and regenerative medicine. J Cell Physiol. 2018;233:5598–612.
62. Zhou Y, Xu J, Luo H, Meng X, Chen M, Zhu D. Wnt signaling pathway in cancer immunotherapy. Cancer Lett. 2022;525:84–96.
63. Waldmann TA. Cytokines in cancer immunotherapy. Cold Spring Harb Perspect Biol. 2018;10:a028472.
64. Li Y, Qian D, Lin H-P, Xie J, Yang P, Maddy D, Xiao Y, Huang X, Wang Z, Yang C. Nanoparticle-delivered Miriplatin ultrasmall Dots suppress triple negative breast cancer lung metastasis by targeting Circulating tumor cells. J Controlled Release. 2021;329:833–46.
65. Xing Y, Xu Y, Chen Y, Jeffrey PD, Chao Y, Lin Z, Li Z, Strack S, Stock JB, Shi Y. Structure of protein phosphatase 2A core enzyme bound to tumor-inducing toxins. Cell. 2006;127:341–53.
66. Sitosari H, Morimoto I, Weng Y, Zheng Y, Fukuhara Y, Ikegame M, Okamura H. Inhibition of protein phosphatase 2A by Okadaic acid induces translocation of nucleocytoplasmic O-GlcNAc transferase. Biochem Biophys Res Commun. 2023;646:50–5.

Publisher's note